THESIS

MODELING EFFECTS OF MICROVILLI ON SOMATIC SIGNAL PROPAGATION

Submitted by

Ahmed A. Aldohbeyb

Graduate Degree Program in Biomedical Engineering

In partial fulfillment of the requirements

For the Degree of Master of Science

Colorado State University

Fort Collins, Colorado

Summer 2018

Master's Committee:

    Advisor: Kevin Lear

    Jozsef Vigh
    Ryan Bailey

ABSTRACT

MODELING EFFECTS OF MICROVILLI ON SOMATIC SIGNAL PROPAGATION

The electrical behavior of small compartments in neurons such as dendritic spines, synaptic terminals, and microvilli has been of interest for decades. Most of these fine structures are found in the dendrite, where most excitatory inputs are received, or in the axon where the action potential is generated and propagates. However, a recent study has shown expression of sodium voltage-gated channels (VGCs) in the soma of intrinsically photosensitive retinal ganglion cells (ipRGCs). Confocal imaging locates these sodium VGCs outside the main soma membrane, which implies that the VGCs occur in structures that protrude from the soma but are too small to be resolved with conventional optical microscopy. An investigator has hypothesized the voltage-gated sodium channels are positioned in microvilli. The microvilli hypothesis raises the question of the role of voltage-gated sodium channels on microvilli and more specifically what effect they would have on propagation of signals in the soma.

The nanoscale dimensions of the microvilli, which are much smaller than patch-clamp probes, prevent conventional electrical studies that isolate individual compartments. In the absence of direct, high-spatial resolution measurements, computational models are valuable tools for developing a better understanding of the electrical behavior of the neuronal compartments. Well known models such as Hodgkin–Huxley models and cable theory have been the foundation of many advances in neuroscience.

In this work, initial insights about the role of somatic microvilli are being generated using an equivalent circuit model based on the cable equation. For the circuit model, microvilli stubs

containing resistor-capacitor networks and sodium channels are treated as branches off the main soma membrane. Circuit models of the soma membrane without microvilli serve as controls. The circuit models were simulated using Simulink. The results show that voltage-gated sodium channels placed on the main soma membrane or on the microvilli increase the amplitude of somatic signals as they propagate to the axon initial segment. Moreover, restriction of the VGCs to the somatic microvilli reduces the probability of misfires originating from spontaneous ion channel opening while still enhancing above threshold depolarizations propagating in the main soma membrane.

For comparison, simulations of somatic signal propagation were also performed using the NEURON software as it readily incorporated the Hodgkin and Huxley model, including both sodium and potassium voltage-gated channels. The dendritic input signal was generated using the current clamp technique. The results show that the presence of VGCs on the main soma membrane lower the threshold for triggering the AIS to generate action potential. However, restricting sodium VGCs to the microvilli only did not initiate an action potential at the AIS. The ability of the microvilli Na^+ VGCs to serve as excitatory inputs directly to the soma in the absence of the dendritic input was also investigated using NEURON. Using a current clamp, current was injected at the tip of the microvilli and the signal was recorded at the AIS. The results show that the signal at the AIS increases linearly with the injected current. However, the amplitude of the AIS potential was lower than the microvilli signal due to the high microvilli neck resistance. The results support the view that the microvilli act as electrical compartments that attenuate the microvilli VGCs' signals.

ACKNOWLEDGMENTS

TABLE OF CONTENTS

LIST OF TABLES

LIST OF FIGURES

CHAPTER 1: INTRODUCTION

1.1 Motivation

Since Cajal's discovery of dendritic spines in the late nineteenth century, the study of fine structures has become one of the most researched topics in neuroscience. Small structures, such as dendritic spines and synaptic terminals, play major role in neuronal physiology, in areas such as action potential generation and synaptic integration. However, the exact role of these fine structures, especially with dendritic spines, is still subject to great debate. The nanoscale dimensions make it challenging to directly measure the electrical behavior of these small neuronal structures, even with the development of nanopipette electrodes. Also, conventional measurement techniques, such as patch clamp, severely distort the measurement on such nanostructures [1]. Thus, computational models have become valuable tools in the development of a better understanding of the electrical behavior of small neuronal compartments.

In neuronal modeling, the soma is usually simplified to be represented by only one segment. One reason for such a simplification is that the soma does not receive any excitatory inputs as excitatory inputs are received onto the dendritic spines. Another reason is that the soma has very low sodium voltage-gated channels (VGCs) expression. However, these assumptions cannot be generalized to all types of neurons. Jozsef Vigh discovered that intrinsically photosensitive retinal ganglion cells (ipRGCs) express voltage-gated sodium channels in the soma. The voltage-gated sodium channels that appear disconnected from the cytoplasm implies that these voltage-gated sodium channels could be positioned in microvilli [2]. Therefore, intrinsically photosensitive retinal ganglion cell' soma needs to be modeled in more detail to account for such observations.

This thesis focuses on the effect of the microvilli on somatic signal propagation. A circuit model is designed based on cable theory. The study investigates the change of electrical behavior with the presence of voltage-gated sodium channel. A computer model was first designed to study the impact of voltage-gated sodium channels placed on the soma versus being placed on microvilli. Subsequently, the model was designed to study the impact of misfiring triggered in a neighboring channel. Then, a second computer model was designed to study the dynamic behavior of the cell, based on the Hodgkin and Huxley model.

1.2 Thesis Organization

This thesis contains five chapters, followed by two appendices. The thesis begins with an introductory chapter with two sections: motivation, and thesis organization. The second chapter is a literature review with 4 sections: background review on neuronal fine structures with a focus on dendritic spines and the current hypotheses about their function; a brief history of neuronal computational models, with two subsections describing in detail the Hodgkin and Huxley model, and the cable model, respectively; a brief information about ipRGCs; significance of this research. The third chapter is the methodology used in this research and it is divided into three sections: an overview, the cable model, and the Hodgkin and Huxley model. The fourth chapter is the results and discussion of the models and is divided into three sections: an overview, circuit models result, and Hodgkin and Huxley model results. The fifth chapter is the conclusions contain two sections: conclusion remarks of each model, and future study.

CHAPTER 2: LITERATURE REVIEW

2.1 Background

There are many studies focused on analyzing the role of neuronal fine structures, such as dendritic spines, beginning with Cajal's work, which was the first study to address the role of dendritic spines. Prior to his work, these fine neuronal structures were thought to be an artifact of Golgi stains. Cajal, on the other hand, argued that these fine structures were not irregular membrane protrusions but rather a spine connected to a ball which is in contact with other neurons[3]. However, the study of neuronal fine structures did not gain much attention until the discovery of electron microscopy, which resolved neuronal fine structure with better spatial resolution[4]. This important invention has opened the door of investigating the role of neuronal fine structures. This led to the first ultrastructural study of synapses in the1950s[5]. Subsequently, E. G .Gray used electron microscopy to prove for the first time that dendritic spines are the site of synaptic contact, which was confirmed later by other scientists[6]. Thus, after these cornerstone discoveries, neuronal fine structures become one of the most researched topics in neuroscience.

Moreover, the exact role of dendritic spines is still under debate. There are different ideas being propagated with regards to the function of dendritic spines. These ideas could be grouped under three different hypotheses [7]. The first hypothesis is that dendritic spines enhance synaptic connectivity. The idea is that the existence of dendritic spines is to increase the interacting area with nearby axons[8], [9]. Experimental data indicate that spines elongate and mediate interaction with the surrounding axons[10].

The second hypothesis is that dendritic spines act as electrical compartments. The high neck resistance of the dendrite, due to its narrow spine, modifies excitatory post synaptic potential

3

(EPSP) [11]–[16]. When a dendritic spine receives an EPSP, the signal is attenuated as it propagates to the parent dendrites, which could have essential roles in neuron plasticity and dendritic integration [15]. One of the electrical advantages of dendritic spines is that they adjust their spine geometry. Which is likely to have an important role in synapse maintenance and development [11]. On the other hand, other studies suggest that spines have a minimal effect on EPSP amplitude [17], while there are also other studies that suggest that dendritic spines have no electrical properties [18][19]. This controversy on the electrical functions of dendritic spine is due to challenges of directly measuring electrical signals on dendritic spine heads [7].

The third hypothesis is that the dendritic spine acts as a biochemical compartment. Dendritic spines have an important role in neuron plasticity. For instance, Calcium accumulation in dendritic spines could allow long term potentiation on individual synaptic input[20], [21]. Moreover, along with their role as a biochemical compartment, dendritic spines could also act as electrical compartments. Therefore, it can enhance plasticity and regulate synaptic strength[7].

2.2 Computational Models

Computational neuroscience has served as a basis which shaped our understanding about neuronal system functions in many aspects. Well known models, such as the Hodgkin–Huxley model and the Cable theory, have been the foundation of many advances in neuroscience because computational models not only predict and interpret experimental data but also provide insights pertaining to the role of key factors of neurons. Such importance stems from the fact that with computational models, the complex geometry of the neuron can be simplified, each factor can be separated, and the various configuration and scenarios can be investigated.

Since the beginning of nineteenth century, neuroscientist have used quantitative models and tried to quantitatively describe how electrical stimulus leads to neuron excitation [22]. This

began with the works of Nernst, who was one of the first scientists to present a quantitative explanation of the neuron membrane excitation phenomena. His equation was used to calculate the potential across the membrane based on the concentration of permeable and impermeable ions. Although the equation prove untenable, scientists took his work as a starting point [23],[22].

In 1907, Lapicque presented his famous Integrate-and-fire (IF) model. He modeled the neuron as a circuit, consisting of a resistor and capacitor in parallel [23]. Lapicque used the model to compute firing frequency in nerve fiber [24]. This model as is still being used and continues to be enhanced. This development ranges from including only a leaky term, to the IF model, to a recent development that Teka et al describes as a Fractional Leaky IF model [25].

All these early works of Nernst, Lapicque, Hill, and others has influenced the work of Hodgkin and Huxley in their famous model [22]. A model proves to be a valuable tool in analyzing and modeling neuronal electrical behavior as it is responsible in shaping our understanding on neuronal electrical behavior.

2.2.1 Hodgkin-Huxley Model

In 1952, Hodgkin and Huxley published a series of papers that mathematically described the initiation and propagation of action potentials in giant squid axon [26]. They observed, by using the model, how the action potential was initiated. They applied a potential that stepped up the resting membrane potential to -9 mV and held the potential there. First, there was a short spike of capacitive current that lasted for a few milliseconds. Then, an influx of sodium ion developed, and the action potential was initiated. When the potential reached its peak value, the sodium conductance dropped to zero, while the potassium ions started to leave the cell slowly. As the potassium ions passed the membrane, the membrane potential moved toward its resting potential value [27].

The Hodgkin and Huxley model consists of capacitor, resistor, and batteries, as shown in Figure 2.1. The capacitor represents the membrane, the resistor represents ion pathway, and the batteries represent the resting potential of each ion species.
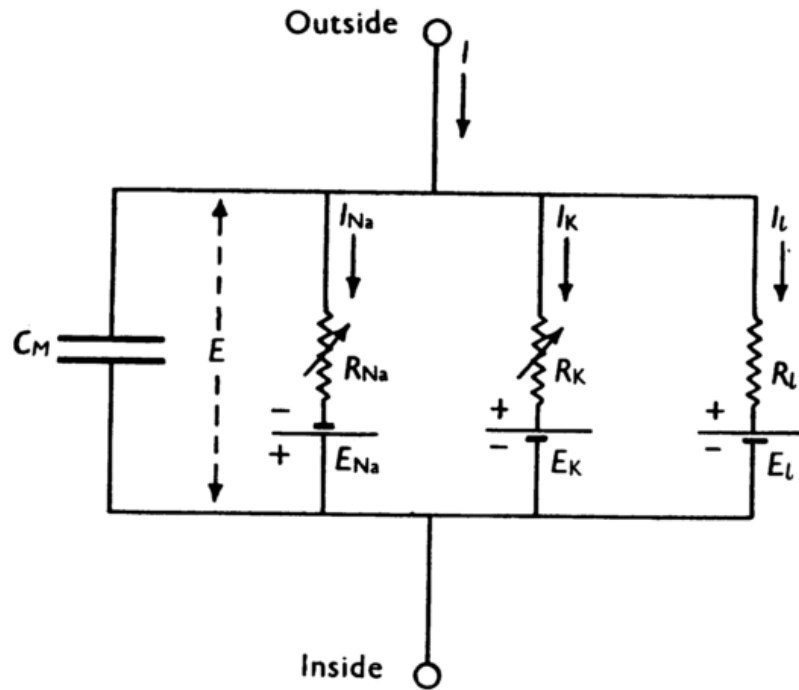
Figure 2.1: Hodgkin & Huxley circuit model (reproduced from Hodgkin & Huxley 1952) [26]

The total current flow through the membrane is the sum of capacitive current and ionic current. Thus,

$$I = C_m \frac{dV}{dt} + I_i$$

Where:

I is the total current

V is the membrane potential

C_m is the membrane capacitance

I_i is the net ionic current

The ionic current can be divided into an algebraic sum of sodium, potassium, and leakage current, as seen in the circuit in Figure 2.1. For each species, the ionic current can be found by ohm law, $I = g_i V$, which could be further expanded to be:

$$I_i = g_i(V - E_i)$$

Where:

g_i is conductance of i ion channel (i: Na, K, or leak)

E_i is the equilibrium potential of i ion

Moreover, Hodgkin and Huxley, along with the total current equation, had expanded their work to include a set of ordinary differential equations to describe the voltage-gated ion channel conductance and its probability to open or close. Therefore, the equation can be summarized as:

$$I = \bar{g}_{Na}m^3(V - E_{Na}) - \bar{g}_k n^4 h(V - E_k) - \bar{g}_l(V - E_l)$$

$$\frac{dn}{dt} = \alpha_n(1 - n) - \beta_n n$$

$$\frac{dm}{dt} = \alpha_m(1 - m) - \beta_m m$$

$$\frac{dh}{dt} = \alpha_h(1 - h) - \beta_h h$$

Where:

$\bar{g}$ is the maximum conductance for i species

α & β are voltage-dependent rate constant

$n, m,$ & h are dimensionless gating variables between 0 and 1

2.2.2 Cable Model

Cable theory was first introduced by William Thomson in 1855. He presented a mathematical model that described the signal decay in submarine telegraph cables. Later, at the beginning of the twentieth century, the cable equation was used to model neuronal core conductance[28].

In a neuron, the cable model was used to study signal propagation and decay along tubular regions of the cell. The spatial temporal distribution of the potential can be expressed with following partial differential equation [28]:

$$\tau \frac{\partial V}{\partial t} = \lambda^2 \frac{\partial^2 V}{\partial x^2} - V$$

Where:

V is the potential

t is the time

x is space

λ is the space constant of the core conductor

τ is the time constant of the membrane

Numerical solution to partial equation requires discretization. This is particularly so when the potential is not uniform along the cable. For instance, when an axon or a dendrite has a tapering diameter, or when the cable contains branches, such as dendritic spines. Thus, the cable must be divided into smaller segments to simplify the complexity of the model. Each segment is composed of a resistance and a capacitance connected in parallel, with an axial resistance connecting the segments together.

The passive cable model with multiple compartments is one the most used model to study the electrical behavior of dendrite, along with the Hodgkin and Huxley model. Both models prove to be an essential tool for study and analysis in many researches in neuroscience, as they are the basic models in neuronal modeling software, such as NEURON and GENESIS.

2.3 Intrinsically Photosensitive Retinal Ganglion Cells

ipRGCs are a type of neuron found in the mammalian retina. It responds to light in the absence of rod and cone photoreceptor inputs. ipRGCs have an important role in mediating the circadian photoentrainment[29]. Also, ipRGCs control the pupil light responses[30]. Moreover, ipRGCs are very important to human health. They have been related to several diseases, such as migraines and sleep disorders [30].

Recently, Jozsef Vigh found sodium voltage-gated sodium channels on ipRGCs soma (Figure 2.2)[2]. The red dots represent panNav antibody labeling which labels sodium voltage-gated channels (NaV 1.1, 1.3, 1.4, 1.5, and 1.7). These clusters of sodium channels appear to be not connected to the cell cytoplasm which is labeled in green, as seen in Figure 2.3[2]. This may imply that these channels are located in some fine structure, like microvilli, that could not be resolved in the images. To the author's knowledge, this is the first-time that voltage-gated sodium channels are described to be expressed on somatic microvilli. Thus, the expression of voltage-gated sodium channels on microvilli raises the question of the role of these channels, especially whether these cluster voltage-gated sodium channels have any impact on somatic signal propagation, and if somatic signal propagation will be affected by the presence of these voltage-gated sodium channels on microvilli.
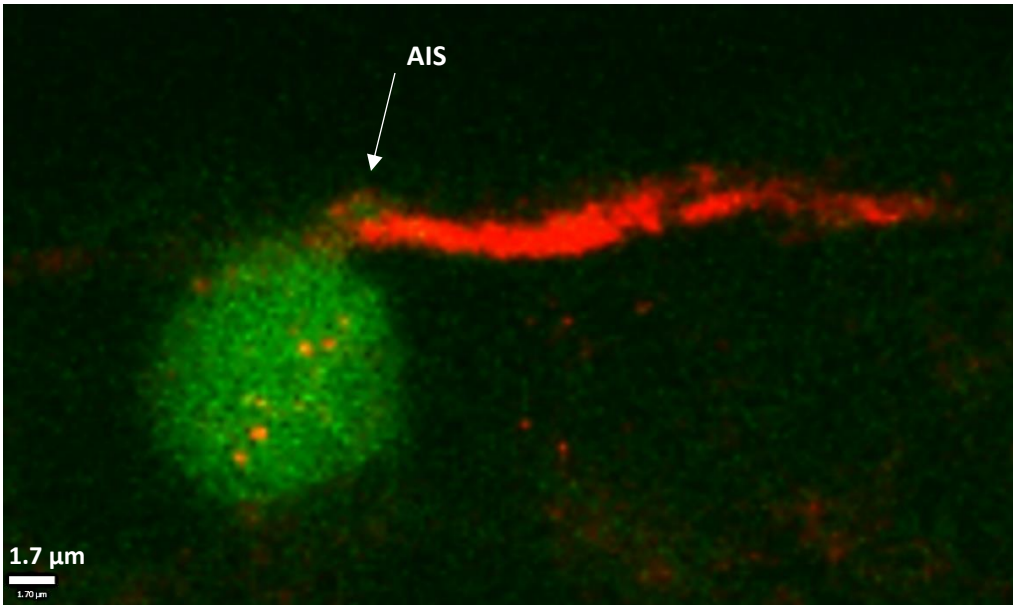
Figure 2.2: Sodium voltage gated channel expression in ipRGCs (courtesy of Jozsef Vigh)
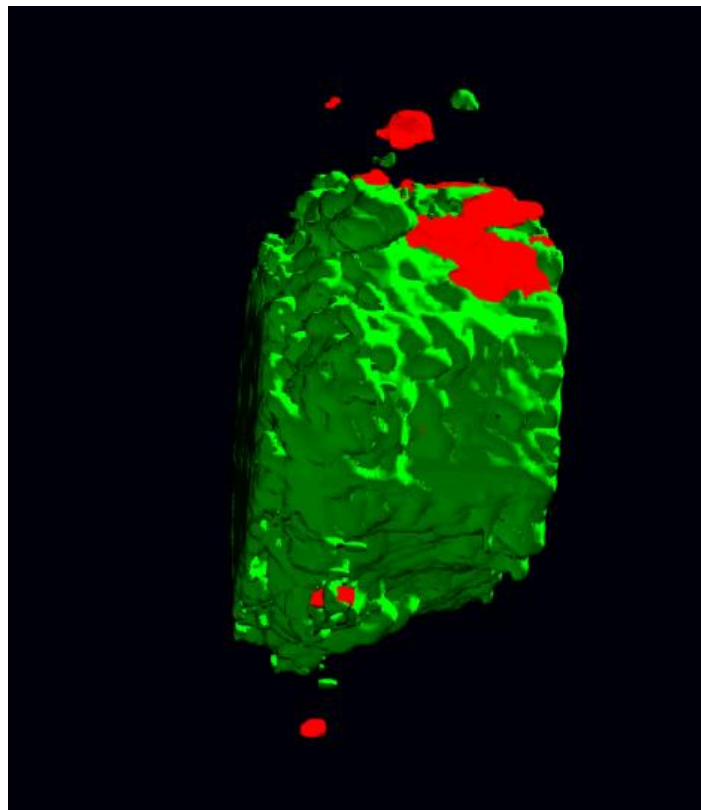
Figure 2.3: Clusters sodium voltage gated channels (red) in ipRGCs soma (courtesy of Jozsef Vigh)

2.4 Significance of This Research

In this work, a circuit model based on cable theory will be applied to analyze ipRGCs' somatic signal propagation in the presence of microvilli, which have not been included before. The circuit model will be varied to study the effect of several parameters, such as soma size and ion channel density. Then, the ipRGCs' somatic signal propagation will be analyzed using the Hodgkin and Huxley model. The dynamic behavior of the model will be studied to compute the threshold, and the microvilli effect on generating an action potential. After that, the two models will be compared, and the conclusions will be summarized.

CHAPTER 3: METHODS

3.1 Overview

In this chapter, a description of the methods used to obtain the results of this research is presented. The theoretical models used to study somatic signal propagation are offered and thereafter, a computer simulation was used to obtain the results. These models were used to study the impact of VGCs in microvilli or the soma shaft on the signal magnitude, threshold, and channel misfiring probability.

3.2 Cable Model

Converting complex geometry and properties of neurons to a simple cable is one of the main purposes of the cable model. It is an effective method to study signal propagation without dealing with the complex neural morphological and physiological properties. Furthermore, its main assumption is to reduce the spatial dependence of the voltage along the cable. Thus, the perpendicular dependence of the voltage can be neglected [28]. Moreover, if the Debye length, L_D, (less than 3 nm) is less than the feature sizes of this model (Equation 3.1), then the sum of the net charges the sum of all ion species with concentration C_i and valence z_i is assumed to be zero, as seen in Equation 3.2, which simplifies the model. Therefore, with such simplification, the neuron can be modeled as a simple circuit, which is shown in Figure 3.1.

$$L_D = \sqrt{\frac{\varepsilon_0 \varepsilon_s K_B T}{q^2 C}} \qquad (3.1)$$

Where:
ε_0 is the relative permittivity of free space
ε_s is the relative permittivity of the solvent
K_B is the Boltzmann constant

T is the absolute temperature in kelvins

q is the charge

C is the concentration

$$\sum_i C_i z_i = 0 \quad (3.2)$$
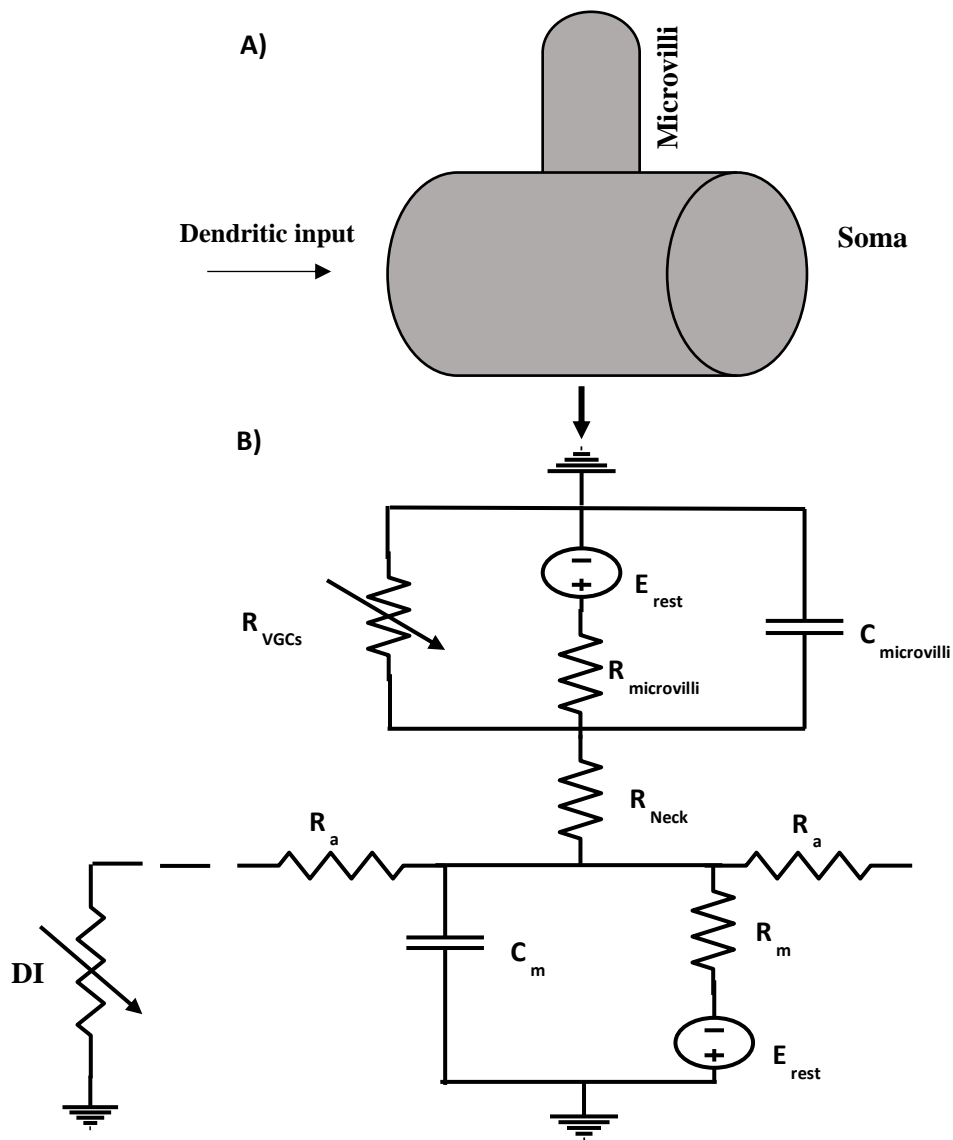
Figure 3.1: A) Diagram of microvilli attached to the soma shaft. B) The microvilli and the soma modeled as an electrical segment attached to each other by R_{neck}. DI represent the dendritic input.

The commercial software used in this section is MATLAB Simulink 2018 [31]. Simulink is a powerful tool that allows the user to design and simulate an electrical circuit with linear and nonlinear components. Moreover, Simulink has the ability to code the function that will control the electrical behavior of certain components, such as variable resistors. This advantage is used to build a variable resistor that will mimic the opening and closing of an ion channel. However, one of the main limitations is that MATLAB Simulink does not allow algebraic loops in the system. This means that a signal exists only with a direct feedthrough block within the loop [31]. Thus, the triggering of ion channels to open or to close cannot depend on the resulting voltage in the system.

3.2.1 Electrical Circuit Model

The lumped equivalent circuit is consistent with cable equation solution. Neuronal morphologies utilized in this model include a portion of the cylindrical axon initial segment, which is 1 µm long and 1 µm in diameter, a cylindrical soma, which is either 10 µm long and 10 µm in diameter, or 40 µm long and 40 µm in diameter, and somatic microvilli, which is 1 µm long and 80 nm diameter. The soma is discretized to 10 segments and one microvilli segment will be attached to the middle of the soma. The values of specific membrane resistance r_m, specific membrane capacitance c_m, and cytoplasmic resistivity ρ were set to 10 KΩ·cm^2, 1 µF/cm^2, and 100 Ω·cm, respectively [11]. The resting potential was set at -80 mV.

3.2.1.1 Input Signal

The input signal in the circuit model for the soma was chosen to mimic the dendritic input. It is represented in the circuit as a variable resistor that behaves as a double exponential function using Equation 3.3 [32]. Further, the maximum conductance, g_{max}, is varied to achieve two goals. The first goal is to generate a potential amplitude similar to the potential amplitude produced from

the dendritic synapse. The second goal is to deliver a certain amount of current to the circuit, such as the peak current value used in a current clamp experiment. Table 3.1 and 3.2 shows the value of g_{max} that produces the desired amount of current or potential amplitude.

$$g = g_{max} \times \frac{\exp\left(-\frac{t}{\tau_f}\right) - \exp\left(-\frac{t}{\tau_r}\right)}{1.3} \quad (3.3)$$

Here τ_r is rise time, and τ_f is the fall time [32]. The input signal was simulated with a rise time of 0.1 ms and a fall time of 1 ms.

Table 3.1: Peak potential amplitude produced from changing the maximum conductance

Potential (mV)	g_{max} (pS)
3.439	0.25
6.709	0.5
12.772	1
23.232	2

Table 3.2: Peak current produced from changing the maximum conductance

Current (pA)	g_{max} (pS)
1	18.65
2	37.3
3	55.98
4	74.68
5	93.4
6	112.2
7	130.97
8	149.76
9	168.57

10	187.4
11	206.25
12	225.12
13	244.01
14	262.92
15	281.85
20	377.4
30	572.1
40	771.2
50	974.5

3.2.1.2 Circuit Parameters

Figure 3.1 presents an illustration of the neuron geometry and its equivalent circuit used in this model. All somatic segments have the same value of resistance and capacitance because the area of each segment is the same. The membrane resistance R_m, capacitance C_m, and the axial resistance R_a were calculated using Equations 3.4, 3.5, and 3.6, respectively. As well, in Equation 3.7, the space constant, λ, in which the signal will decay $1/e$ of its original amplitude [33]. Table 3.3 shows the value of each element in the circuit.

$$R_m = \frac{r_m}{2\pi a L} \quad (3.4)$$

$$C_m = 2\pi a L c_m \quad (3.5)$$

$$R_a = \frac{\rho L}{2\pi a^2} \quad (3.6)$$

$$\lambda = \sqrt{\frac{r_m d}{4 r_a}} \quad (3.7)$$

Where

a is the radius

d is the diameter,

L is the segment length

Table 3.3: Circuit model parameters

Part	Segments	L (μm)	a (μm)	R_m (GΩ)	C_m(pF)	R_a(MΩ)
1) 40 μm x 40 μm Soma	10	4	20	1.99	5.02	0.003
2) 10 μm x 10 μm Soma	10	1	5	31.83	0.31	0.012
Microvilli	1	1	0.04	3.98×10^3	2.51×10^{-3}	200
Axon Initial segment	1	1	0.50	3.18	3.14×10^{-2}	1.27

To investigate the impact of the microvilli axial resistance, R_{neck}. The model was simulated with several values for this parameter. The microvilli neck resistance was adjusted by changing the cytoplasmic resistivity or the microvilli radius. The values used in this model were 200 MΩ, 500 MΩ, and 1 GΩ, which are in the range of the most used values for neck resistance in dendritic spines models [1], [11], [34], [35].

3.2.2 Signal Boosting

Investigating the effect of somatic sodium VGCs on the signal amplitude is one of the goals of this research. Somatic sodium VGCs in this model will be time triggered, as the MATLAB Simulink does not allow for an algebraic loop, which means the VGCs cannot be voltage triggered. However, because the space constant, $\lambda = 1.58$ mm, is much larger than the length of the soma ($L = 10$ μm), the VGCs will be triggered nearly instantaneously with the input signal.

To measure the output signal amplitude at the axon initial segment (AIS), both the input signal and the sodium VGCs are initiated at the same time, and the output is measured at AIS. Na$^+$

VGCs are modeled using Equation 3.1. For the maximum conductance of single channel Na^+ VGCs, previous studies reported different values ranging from 8 pS to 24 pS [36][37] [38]. In this model, the maximum conductance for a single channel was set to 24 pS. Then, the number of channels was varied between 1 to 40 channels. Also, one simulation was run with 8 pS for a single channel to cover the smallest value reported for a single sodium channel [36]. Moreover, varying the number of channels over a range up to 40, will produce a maximum conductance in the microvilli that is about 5 times higher conductance of Na^+ VGCs density of retinal ganglion cell somas [39]. In other words, using Equation 3.8, the maximum conductance, g_{max} produced is 1.02 nS, which is approximately the value of 40 Na^+ VGCs, 0.96 nS. Thus, the effect of Na^+ VGCs signal will be investigated from the smallest to the highest amplitude that might be generated.

$$g_{max} = (5 \times Na^+ \text{ VGCs density}) \times \text{Microvilli surface area} \qquad (3.8)$$

Further, the effect of the Na^+ VGCs position on signal propagation is studied with VGCs either positioned on microvilli or on the soma shaft, while the output is measured at the AIS, as seen in Figure 3.2 and 3.3. When the model is simulated with Na^+ VGCs positioned on the microvilli or the soma, the VGCs are connected in parallel with the membrane resistance and capacitance and in series with the axial resistance.
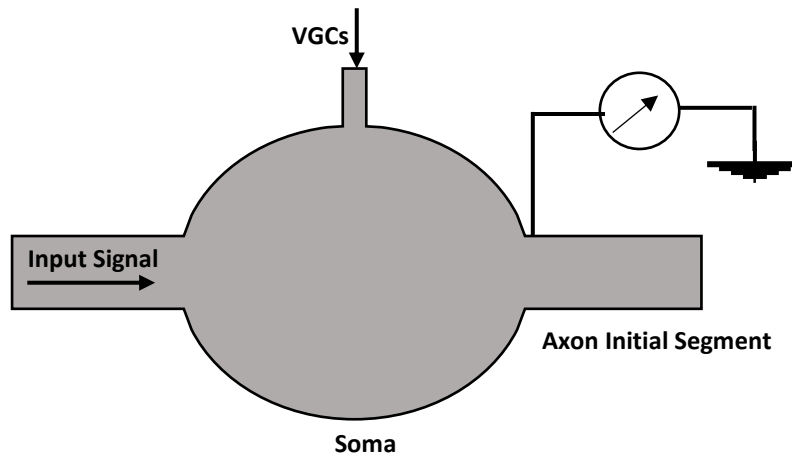
Figure 3.2: Signal amplitude simulation with VGCs positioned on the microvilli.
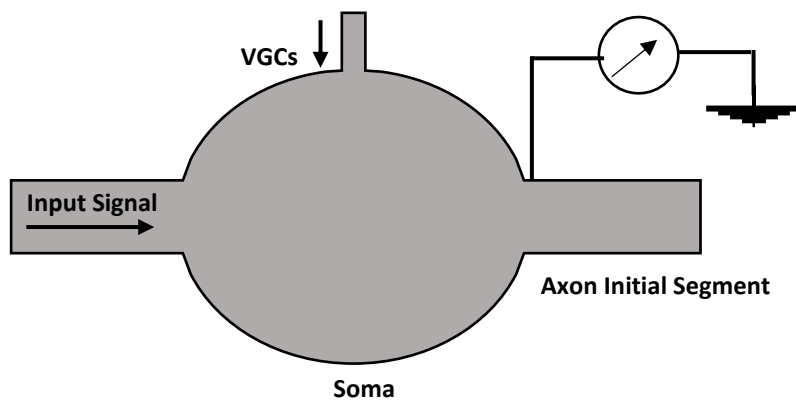
Figure 3.3: Signal amplitude simulation with VGCs positioned on the soma shaft.

3.2.3 Misfiring Model

The second simulation in the circuit model is to investigate the probability of misfiring. VGCs operate stochastically which means that the channel always fluctuates between the open and close state. The idea is to investigate the probability that VGCs in one microvilli can trigger another cluster of VGCs in neighboring microvilli in the absence of a dendritic stimulus. The potential at the first microvilli neck is recorded with only a simulated dendritic signal. Then, the value of the microvilli potential is recorded with only VGCs on neighboring microvilli generating a signal. Figure 3.4 illustrates the misfiring simulation.
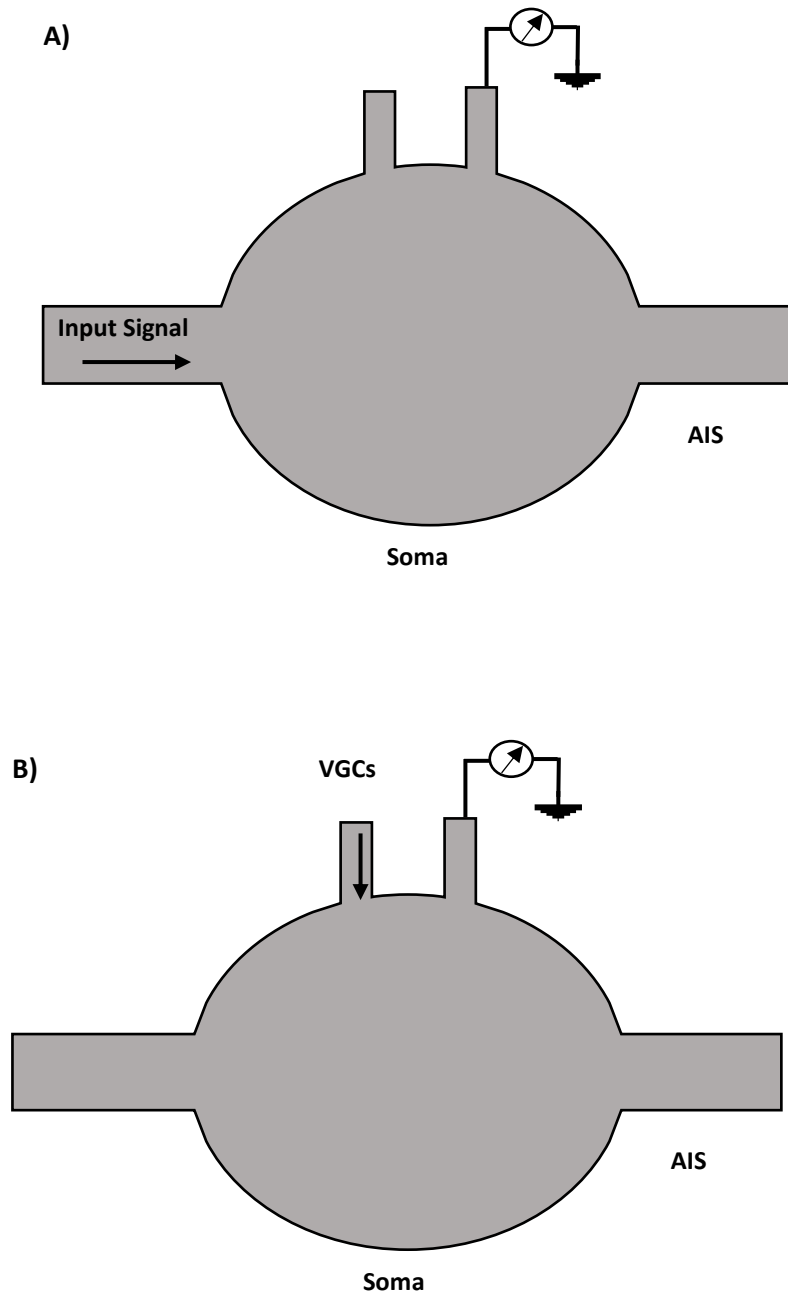
Figure 3.4: Misfiring simulation. A) Potential recorded at the microvilli, resulting from a dendritic signal. B) Potential recorded at the microvilli, resulting from a signal generated from neighboring microvilli.

3.2 Hodgkin-Huxley Model

As described, the HH model is a mathematical model that incorporates sodium and potassium VGCs [26]. The commercial software used for simulations including the complete HH

model is NEURON 7.5 [40]. It is one of the most used programs in neuroscience. It is a simulation environment to model single neuron and neuronal networks. One advantage of using NEURON is the built-in HH model that allows the ion channel to be voltage triggered, where the ion channels could be passive ion channels that are always open, or HH ion channels properties.

The neuronal morphology utilized in this model is the same morphology used in the previous model, with only two differences. First, in this model, only 10 µm x 10 µm soma were modeled. Secondly, one cylindrical dendrite segment that was 1 µm long and 5 µm in diameter was created to position a current clamp electrode, along with an axon initial segment (AIS) that was 1 µm long and 1 µm in diameter, where the output signal is measured. A current clamp technique was used to stimulate the neuron. In the current clamp technique, the current is injected by an electrode into the cell, and the same electrode also measures the membrane potential caused by the injected current. In this model, the current was injected to the dendritic segment unless otherwise stated. The current is injected for 10 ms after running the simulation for 100 ms. This waiting period is suggested by NEURON to ensure that each compartment is close to its resting potential values. The simulation was run for 300 ms to give enough time for the membrane to relax back to the resting potential value. Table 3.4 shows the current amount injected and its resulting potential amplitude.

Table 3.4: Input potential amplitude resulting from current injections

Current (pA)	V (mV)
0	-80.0000
1	-78.1034
2	-76.2074
3	-74.3110
4	-72.4139

5	-70.5155
6	-68.6150
7	-66.7107
8	-64.8002
9	-62.8793
10	-60.9415
11	-58.9765
12	-56.9689
13	-54.8958
14	-52.7238
15	-50.4058
20	-34.1593
30	-5.04815
40	12.0152
50	29.0031

3.2.1 Signal Boosting

Studying the effect of VGCs on the signal and determining the threshold potential of Na^+ VGCs are the goals of this experiment. VGCs are positioned either on the soma, the microvilli or both. The simulation is run two times, one with Na^+ and K^+ VGCs and the other with only the Na^+ VGCs to study the effect of Na^+ VGCs with the absence of any K^+ VGCs. Moreover, these are compared with the results obtained from the MATLAB Simulink simulation. In this model, the dendrite was created with passive properties, while the soma, microvilli, and axon initial segment were modeled with HH properties. The density of the Na^+ and K^+ VGCs were adopted from the values reported in the retinal ganglion cells [39]. These values are listed in Table 3.5. In addition to the listed values, the VGCs' density in the soma and microvilli were varied to measure the

triggering threshold of Na$^+$ VGCs' and to investigate how the signal at the AIS was affected. Table 3.6 shows the channel density used in this simulation.

Table 3.5. Distribution of ionic channels

Channel	Soma & Microvilli (mS/cm^2)	Axon Initial Segment (mS/cm^2)	Reversal Potential (mV)
Na	80	150	35
K	18	18	-75
Leak	0.0001	0.0001	-80

Table 3.6. Ionic channel densities used in the model

Simulation	Na (mS/cm^2)	K (mS/cm^2)
1	0	0
2	5	2.25
3	10	4.5
4	40	9
5	80	18
6	160	36
7	240	54
8	320	72

The number of microvilli was increased to 2, and to 4 microvilli, in order to study how they might influence somatic signal propagation. The first model contains two microvilli that are located 2 µm apart and attached to the middle of the soma. The second model contains 4 microvilli that are located 2 µm, 4 µm, 6 µm, and 8 µm from the AIS. Both models were simulated two times, one with Na$^+$ and K$^+$ VGCs and the other with only the Na$^+$ VGCs.

3.2.2 Current Clamp on Microvilli

The goal of this simulation is to investigate the effect of the signal being initiated at the microvilli. Thus, the VGCs are only expressed on the microvilli and the effect of the presence of both ionic channels versus only Na$^+$ VGCs are investigated. The densities of Na$^+$ and K$^+$VGCs was set to 80 mS/cm^2, and 18 mS/cm^2, respectively.

In NEURON, the current clamp electrode will always be positioned to the middle of the segment. Therefore, if only one segment was used for the microvilli, the electrode will be positioned 0.5 µm from the soma shaft and not at the top of the microvilli. Thus, the microvilli was modeled with four equal segments and the electrode was placed on the fourth segment that represents the top of the microvilli. The amount of the current that was injected into the microvilli and the resulting input signal amplitude at the microvilli is presented in Table 3.7.

Table 3.7: Current amount injected into the microvilli and its input potential amplitude

Current (pA)	amplitude (mV)
1	2.0707
2	4.1403
3	6.2106
4	8.2816
5	10.3538
6	12.4283
7	14.5064
8	16.5906
9	18.6855
10	20.7972
11	22.936
12	25.1175
13	27.3644
14	29.7102
15	32.2019
20	49.3573
30	80.16805
40	98.9704
50	117.6971

CHAPTER 4: RESULTS

4.1 Overview

In this chapter, the results of the models are presented. The results of the electrical behavior of the somatic signal in the presence of VGCs on microvilli are presented and compared with the results of the presence of VGCs on the soma shaft. The results of VGC misfiring on microvilli are also presented.

4.2 Cable Model

The circuit model was analyzed and simulated to study the electrical behavior of somatic signals in the presence and absence of microvilli. Four factors have been investigated in this model: (1) the amplitude of the signal input, (2) neck resistance, (3) the number of VGCs, (4) the soma size (comparing a 10 µm x 10 µm soma to a 40 µm x 40 µm soma). In addition, two experiments have been investigated in this model: the probability of misfiring , and the output from injecting different current amounts.

4.2.1 Signal Boosting

Considering the circuit model in Figure 3.1, based on the cable equation, the simulation was repeated 4 times for each dendritic input. Each dendritic input signal was obtained by changing the input maximum conductance as shown in Figure 4.1. The simulation was run with VGCs positioned on the microvilli and the VGCs maximum conductance was set to 24 pS for single sodium VGCs. The number of channels was set to 10 VGCs.
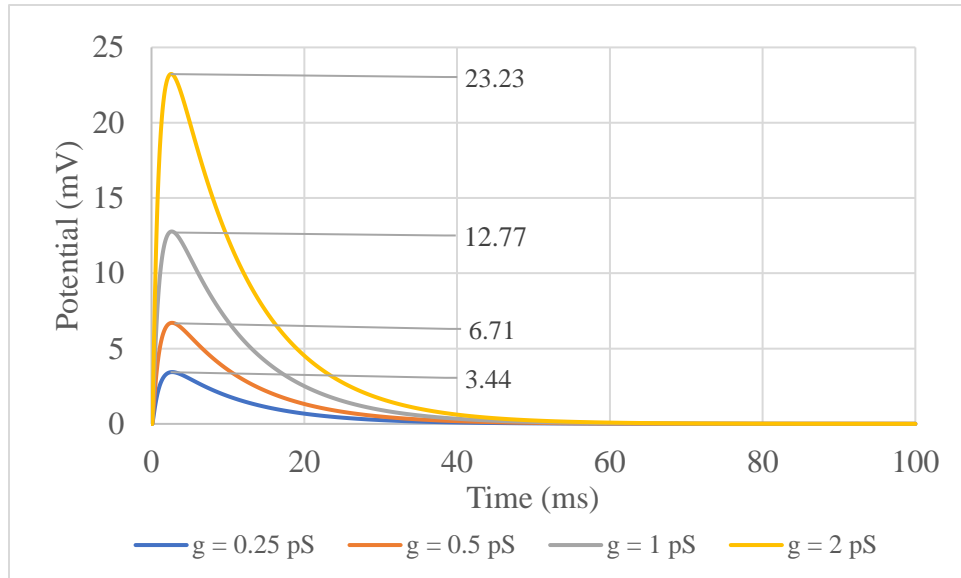
Figure 4.1: Different dendritic input signals are obtained by changing g_{max} in Eq 3.1.

First, the output signal was measured at the AIS with only the dendritic input signal, omitting somatic VGCs from the model (Figure 4.2). As expected, there was no difference in the amplitude between the dendritic input and the AIS signals since the soma length, $L = 10 \ \mu m$, is much smaller than the space constant, $\lambda = 1.58 \ mm$, in which the signal amplitude decays 37%. Also, because the soma length is much smaller than the space constant, there was no change in the signal shape. Therefore, the only difference between the input and the output signals is the peak value. So, in the following sections, the signal peak value is referred to as the signal amplitude.
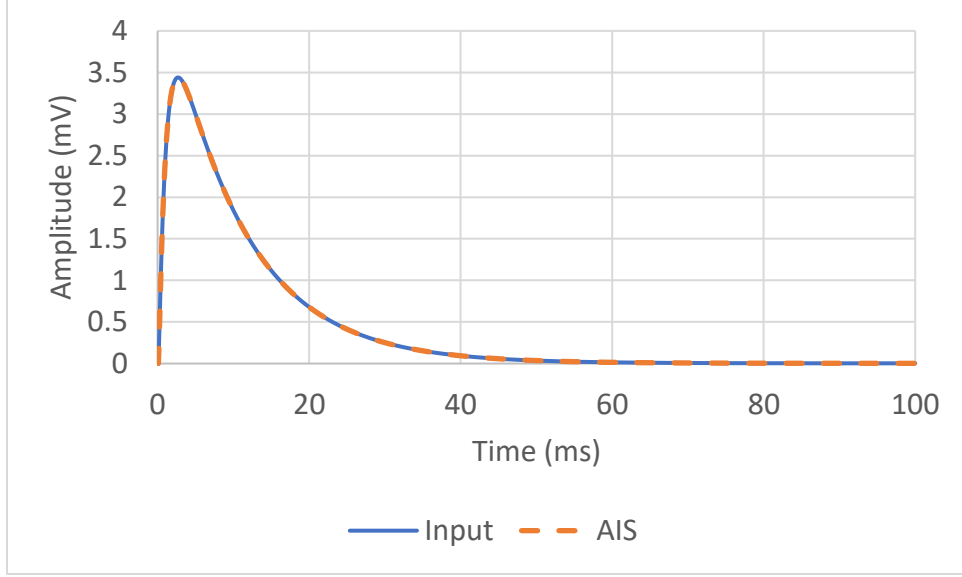
Figure 4.2: Output signal at AIS with 3.44 mV input signal.

Then, the output signal was measured at the AIS with the presence of 10 VGCs on the microvilli. The VGCs were triggered at the same time the dendritic input was generated, as described in section 3.2.2. As seen in Figure 4.3, 4.4, 4.5 and 4.6, the VGCs boosted the output amplitudes at the AIS compared to the AIS amplitudes without any VGCs. The dependence of the output signal on the dendritic input and VGCs can be expressed using Equation 4.1, which shows the increase in the AIS's amplitude is additive rather than multiplicative. Therefore, the effect of the VGCs is most significant with smaller dendritic signals, as the VGCs' impact on the AIS amplitude decreases as the dendritic signal increases. For example, the AIS amplitude increased 89.5% a with 3.44 mV input signal, while it only increased 9.4% with the 23.23 mV input signal. Thus, VGCs will have a higher impact on smaller dendritic signals as it propagates to the AIS.

$$\Delta V_{AIS} = \Delta V_{DI} + N_{VGCs} \times \Delta V_{single\ VGCs} \quad (4.1)$$

Where:

ΔV_{AIS} is the output peak value at the AIS

ΔV_{DI} is the dendritic input peak value

N_{VGCs} is number of VGCs

$\Delta V_{single\,VGCs}$ is the peak value of a single VGC
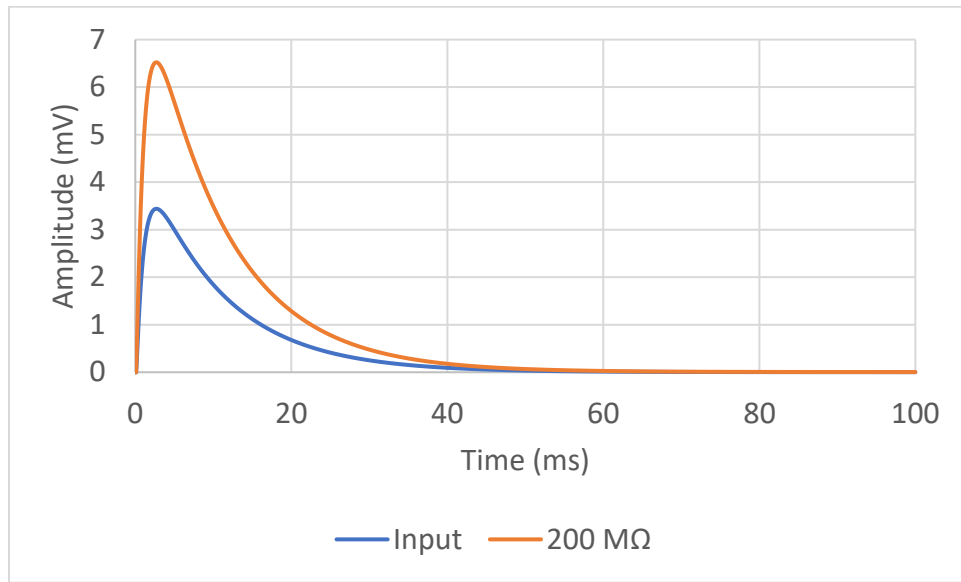
Figure 4.3: Output signal at AIS with 3.44 mV input and 10 VGCs.
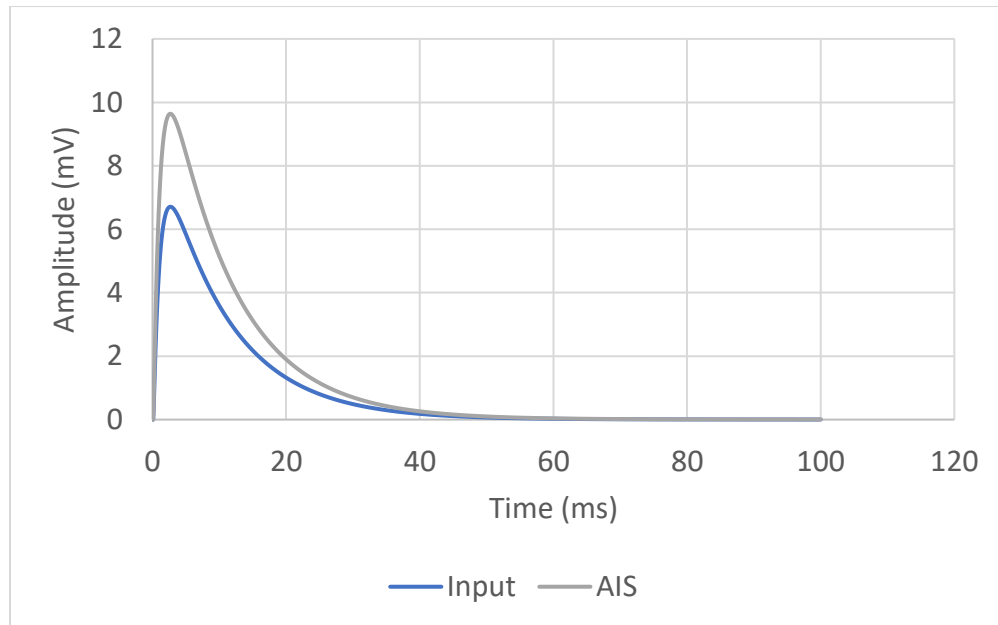
Figure 4.4: Output signal at AIS with 6.71 mV input and 10 VGCs.
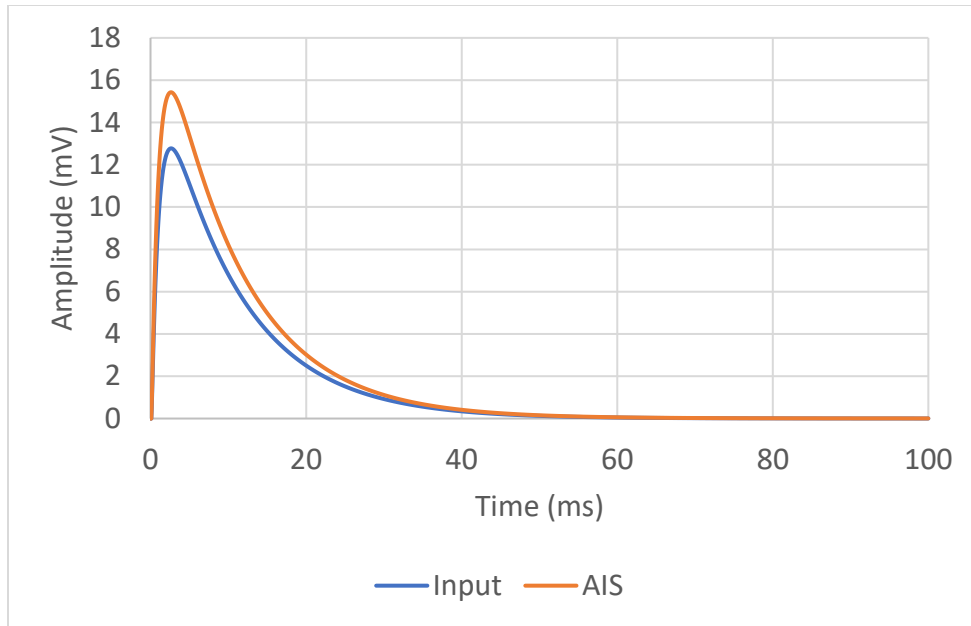
Figure 4.5: Output signal at AIS with 12.77 mV input and 10 VGCs.
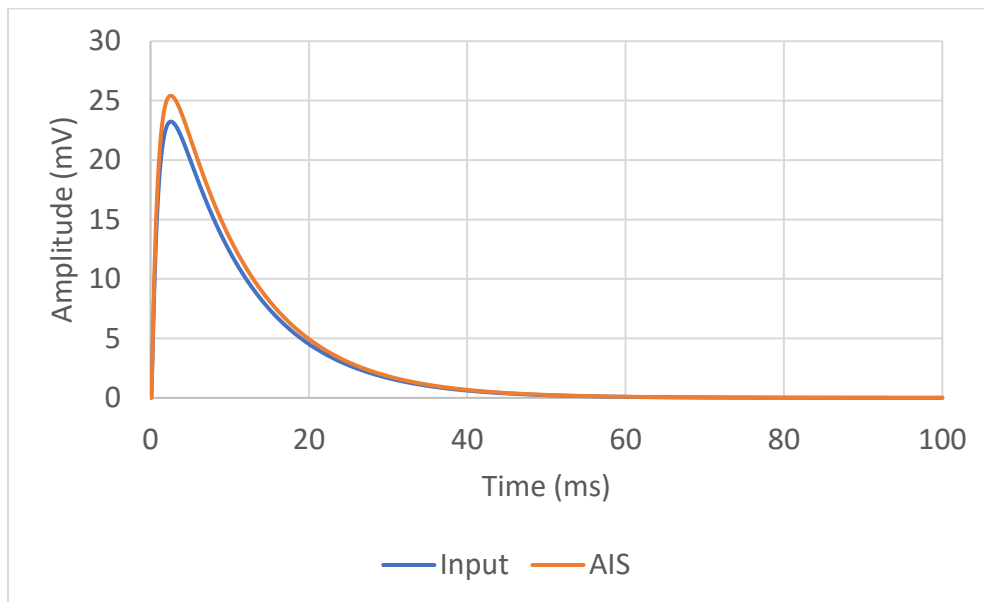
Figure 4.6: Output signal at AIS with 23.23 mV input and 10 VGCs.

4.2.2 Voltage-Gated Channel's Density

The number of channels in the microvilli were varied between 1, 5, 10, 20, and 40 channels to see the effect of the number of channels on the AIS' amplitude. As shown in figure 4.7, equation 4.1 very closely approximates the results obtained from the circuit model. When the amplitude of

29

a single VGC was set between 0.193 mV for ΔV_{DI}= 3.44 mV and 0.273 mV for ΔV_{DI} = 23.23 mV,

the AIS's amplitude results obtained from the equation matches the circuit model results with less

than 5% difference. The good agreement shows that the output signal amplitude increases linearly

with the number of VGCs, and the percent increase in the AIS amplitude depends on input

amplitude as seen in Figure 4.8. For example, increasing the number of channels amplified the

somatic signals as it propagates to the AIS. The highest additive increase, with 40 VGCs, occurs

with the smallest dendritic input, with more than a 3 folds increase. Further, the lowest increase,

33%, happened with 23.23 mV dendritic input. Moreover, the same effect mentioned in Section

4.2.3 that had the highest impact is the most significant with smaller input signals.
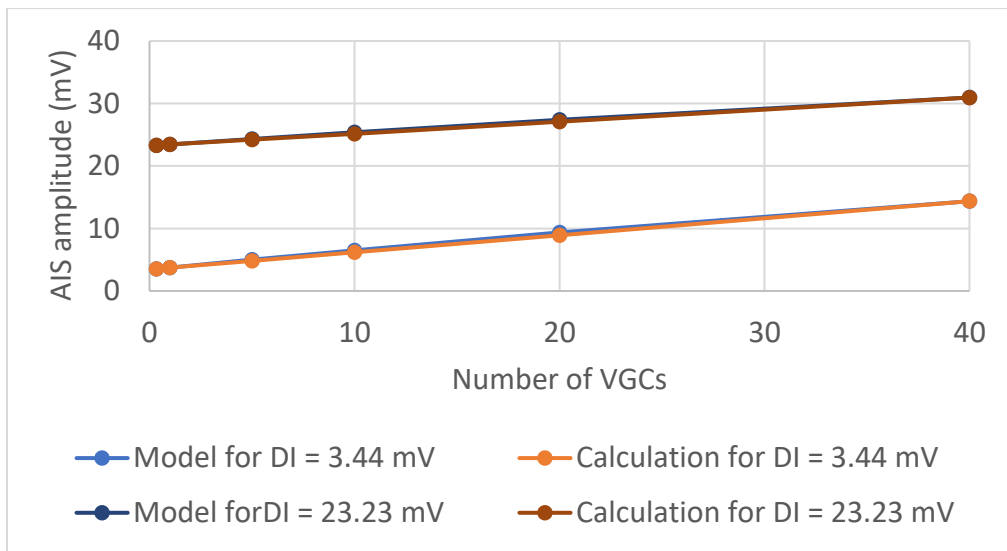
Figure 4.7: Output amplitude at AIS with different input signals versus number of VGCs. model lines in the graph represent the value obtained from the circuit model, and Calculation lines represent the values obtained from Eq 4.1.
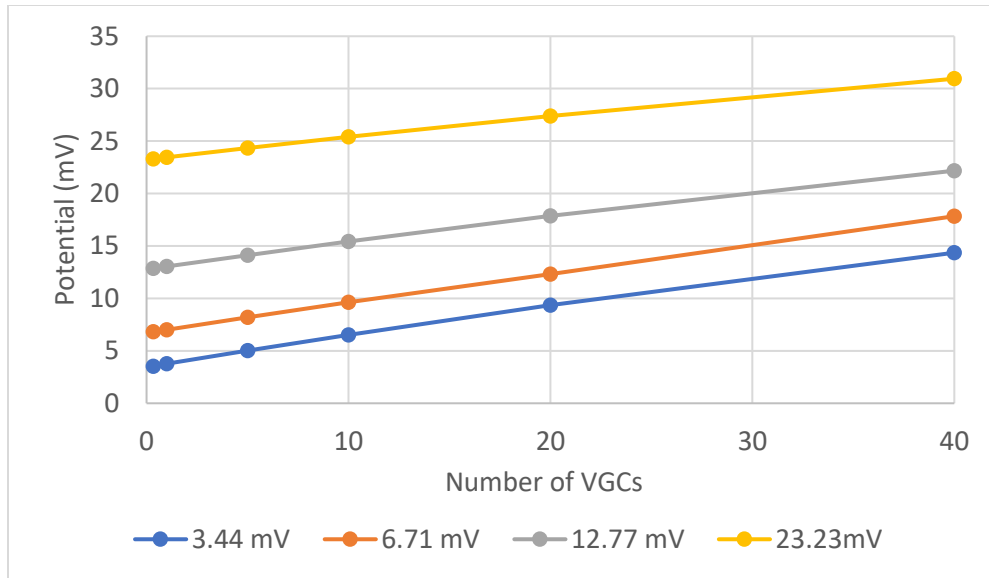
Figure 4.8: Output amplitude at AIS with different input signals versus number of VGCs.

4.2.3 Voltage-Gated Channel's Position

Investigating whether somatic microvilli have an effect on somatic signal propagation is one of the main goals of this research. Some previous studies on dendritic spines have demonstrated that the output signal is highly impacted when the synapse is placed on the dendritic spine [11], [34], [41], whereas other studies have shown that placing synapses on spines has the same electrical effect as if the synapse is placed on the dendrite shaft [19]. Therefore, the position of VGCs is being investigated and analyzed to determine if the microvilli have an impact on the signal.

In the circuit model, the position of the VGCs has an insignificant effect on somatic signals. As shown in Figure 4.9, there is minimal difference in the amount of signal boosting by putting the VGCs on the soma membrane or in microvilli. For instance, the AIS signal is boosted at most to 1.75%, a 60 μV, difference in amplitude between placing 10 VGCs on the soma shaft compared to placing it on microvilli. Even when the number of channels was increased to 40 VGCs the AIS amplitude with the VGCs positioned on the soma increased the AIS' amplitude less than 0.79 mV,

compared to the AIS' amplitude when the VGCs are positioned on the microvilli (results in Table 4.1). This small difference of the VGCs' signal placed on the microvilli is because of the high microvilli neck resistance, 200 MΩ, compared to the soma axial resistance, 12.7 kΩ. Thus, there is neither a significant advantage nor disadvantage of having VGCs on microvilli on boosting AIS's amplitude.
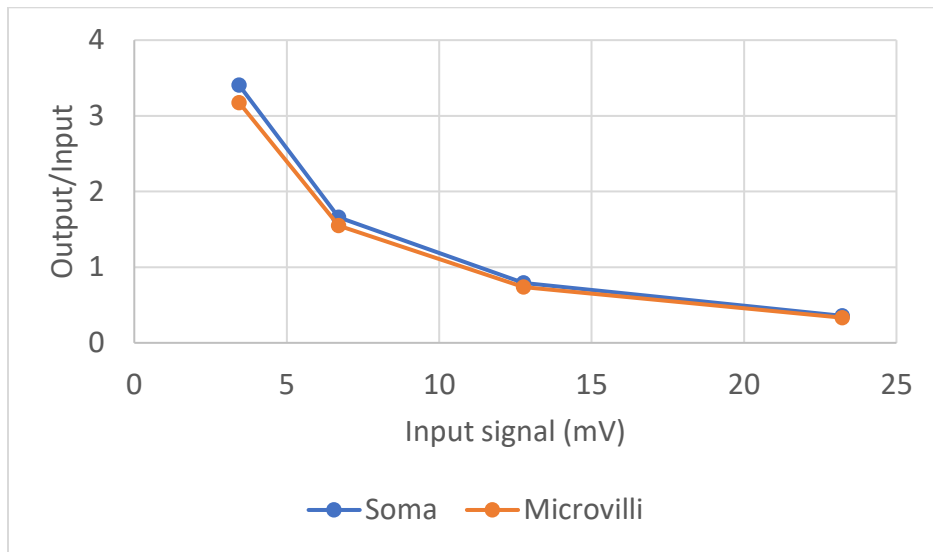
Figure 4.9: Normalized output signal increase percent with 40 VGCs placed on the microvilli or soma.

Table 4.1: Output amplitude at AIS with 10, 20, and 40 VGCs placed on the soma shaft or microvilli, where N is the number of VGCs, and DI is the dendritic input.

N DI	Soma (mV)			Microvilli (mV)		
	10	20	40	10	20	40
3.44	6.58	9.57	15.15	6.52	9.35	14.36
6.71	9.7	12.54	17.84	9.64	12.33	17.1
12.77	15.48	18.05	22.18	15.43	17.86	22.85
23.2	25.45	27.56	31.51	25.41	27.4	30.95

4.2.4 Neck Resistance

A similar approach was taken to study the impact of neck resistance on the electrical behavior of somatic signal propagation. Neck resistance plays a major role in the electric behavior in dendritic spines [42][11]. The high neck resistance acts as an electrical compartment that attenuates the signal. Thus, since the value calculated in this model is equal to the value reported for dendritic spine, the effect of the microvilli neck resistance has been studied in this research. The values of neck resistance used in this simulation are 200 MΩ, 500 MΩ, and 1 GΩ, which are in the range of the most used values for neck resistance in dendritic spines models [1], [11], [34], [35].

Increasing microvilli neck resistance, R_{Neck}, makes the VGCs in the microvilli less effective at boosting the output signal at the axon initial segment. As the R_{Neck} increases, more potential is dropped across the neck. As shown in Figure 4.10, with 200 MΩ, the output decreased 1.75% compared to VGCs on the soma shaft, while it decreased 8% when the neck resistance was set to 1 GΩ. Thus, this is similar to the observations made on increasing dendritic spines' resistance, which reveals that increasing R_{Neck} reduces the amplitude of somatic signals [17]. Similarly, if the number of VGCs increases to 40, R_{Neck} reduces the amplitude boosting compare to VGCs on soma. As shown in Figure 4.11, VGCs on soma boosted the signal 11.7 mV as it propagates to the AIS, while when VGCs on microvilli with 1 GΩ, the AIS amplitude increased only 8.75 mV.
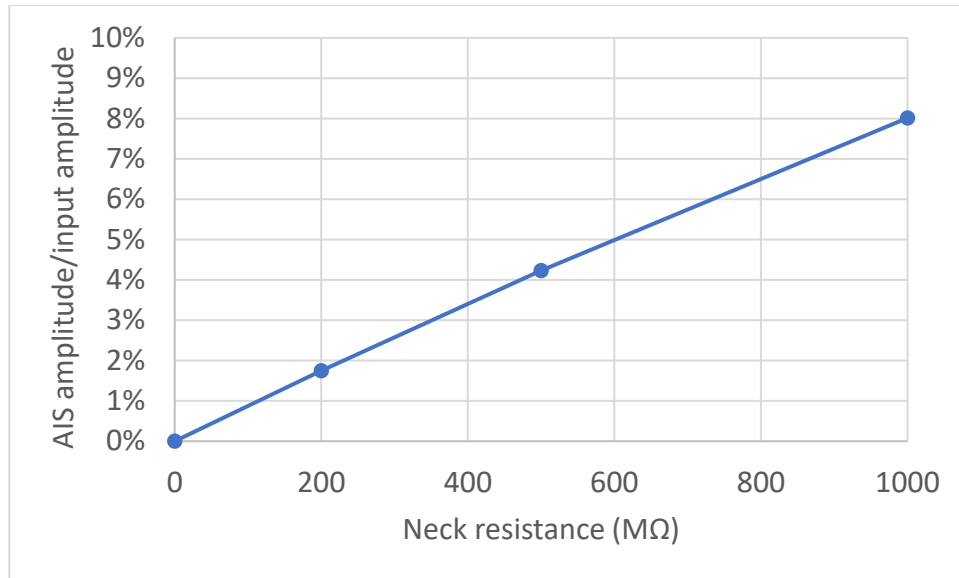
Figure 4.10: Output signal versus different R_{Neck} values with 10 VGCs.
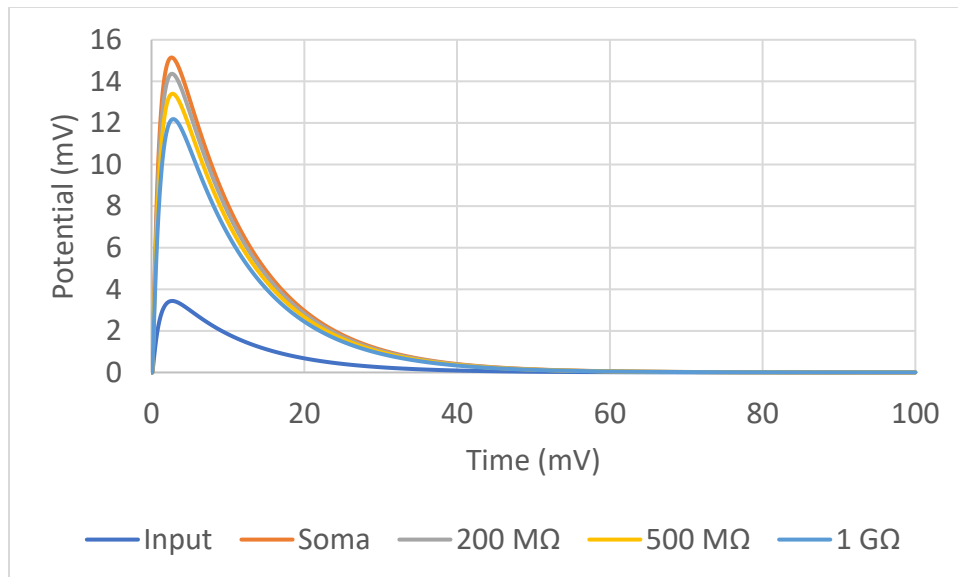
Figure 4.11: Output signal versus different R_{Neck} values with 40 VGCs.

4.2.5 Probability of Misfiring

The opening and closing of VGCs operate stochastically [43], while the ion channel is always fluctuating rapidly between an open and closed state [44]. When the membrane potential near the VGCs randomly depolarizes and thus the probability that the ion channel could open

increases, the VGCs could misfire even without any stimuli from the dendrite. Therefore, having VGCs on the microvilli with a high R_{Neck} could prevent random openings of those VGCs causing misfiring in the soma by reducing the VGCs signal. A model was designed as described in section 3.2.3 to study and analyze VGCs' misfiring.

The relative probability of a VGC in a microvilli misfiring was examined for the case of an input signal coming from another microvilli on the soma compared to a baseline of the input signal coming from the dendrite. In particular, the amplitude of the signal at the receiving microvilli was measured when the dendritic signal comes only from the dendrite and compared to the case when the signal input comes from a neighboring microvilli's VGCs. The amplitude of the signals at the receiving microvilli was obtained for each value of R_{neck} (Table 4.2). Neck resistance has an insignificant effect, with less than 5 μV between 200 MΩ and 1 GΩ on amplitude values at the microvilli with the signal coming from the dendrite. This is because the current will primarily flow into the lower soma axial resistance, 12.7 KΩ, rather than the high microvilli neck resistance. However, notably, the values of the amplitude resulting from VGCs misfiring is smaller than the values obtained from dendritic input signals. The amplitude of the signal at the neighboring microvilli with 1 GΩ was reduced by 25% of the 40 VGCs' signal amplitude. Therefore, the microvilli could prevent misfiring if the threshold to trigger the opening of the VGC is in the appropriate range to trigger AIS (Figure 4.12, and 4.13).

**Table 4.2: Comparison between the amplitude at microvilli with and without dendritic input at different neck resistance**

R_{neck}(MΩ)	Microvilli to microvilli			Dendritic input to microvilli		
	1 VGCs (mV)	10 VGCs (mV)	40 VGCs (mV)	3.4392 (mV)	6.7085 (mV)	12.7729 (mV)
0	0.3363	3.3029	12.3028	3.4393	6.7086	12.7731

200	0.3373	3.2393	11.4805	3.4391	6.7083	12.7724
500	0.3362	3.1493	10.4721	3.4388	6.7078	12.7713
1000	0.3345	3.013	9.1966	3.4384	6.7069	12.7697
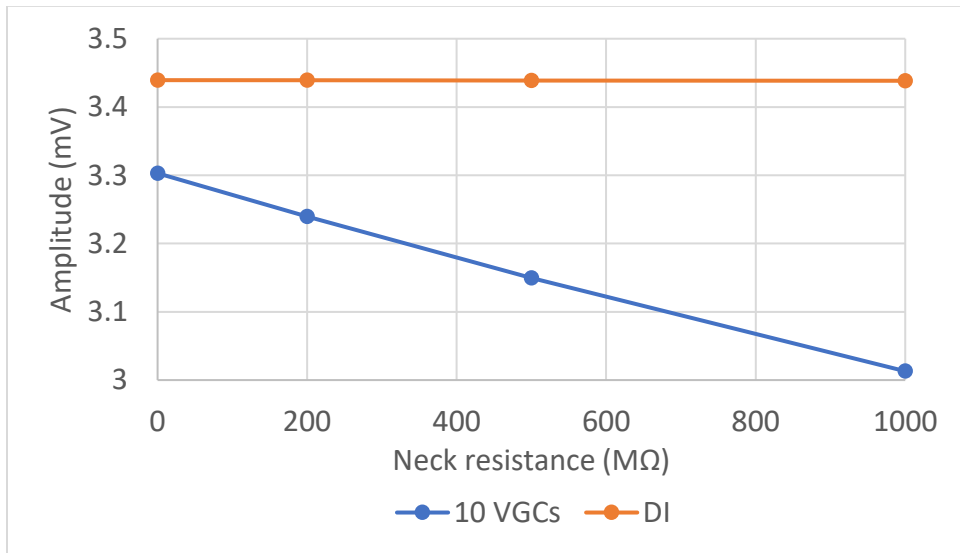
Figure 4.12: Signal amplitude at the microvilli with only dendritic input, DI, and with only 10 VGCs on the microvilli.
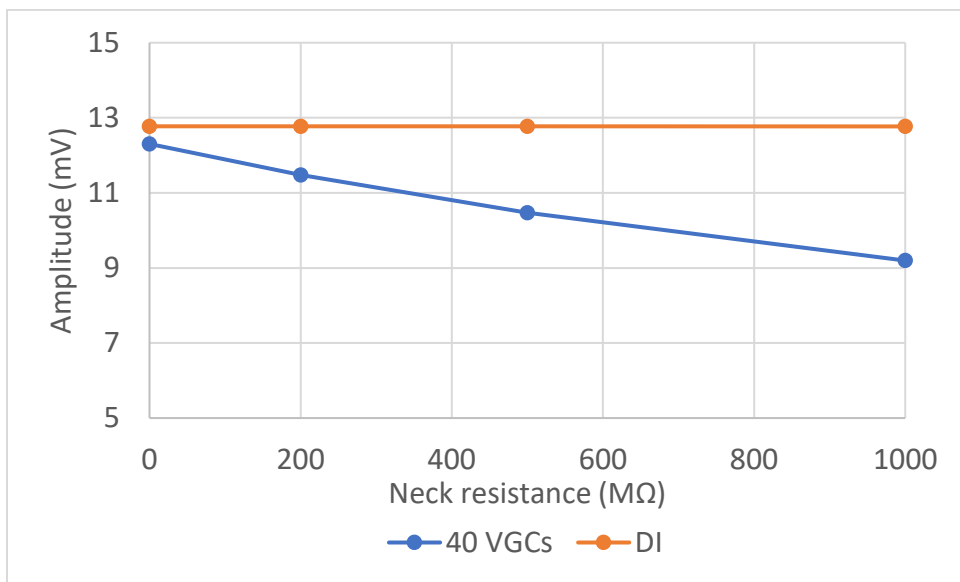
Figure 4.13: Signal amplitude at the microvilli with only dendritic input, DI, and with only 40 VGCs on the microvilli.

4.2.6 Current Clamp

The maximum conductance in Eq 3.1 was varied to correlate the amplitude of potential changes at the AIS changes with different amounts of current injected at the dendrite. The signal was generated by changing the maximum conductance of the variable resistor on the dendrite-soma junction. This simulation was run to compare the results obtained from the circuit model with the results from NEURON's Hodgkin-Huxley model since the circuit model uses a variable resistor input and NEURON uses a current pulse input. As expected, the amplitude at the AIS increased linearly with the increase of the current amount, as seen in Figure 4.14. The linear increase of AIS amplitude with the injected is determined by the membrane capacitance. For example, in figure 4.14, the slope of the two lines is approximately 3.9×10^{-12}, which is approximately the value of the soma membrane capacitance 3.2 pF. This indicates that below the threshold, the model will have a linear response to the amount of current injected.
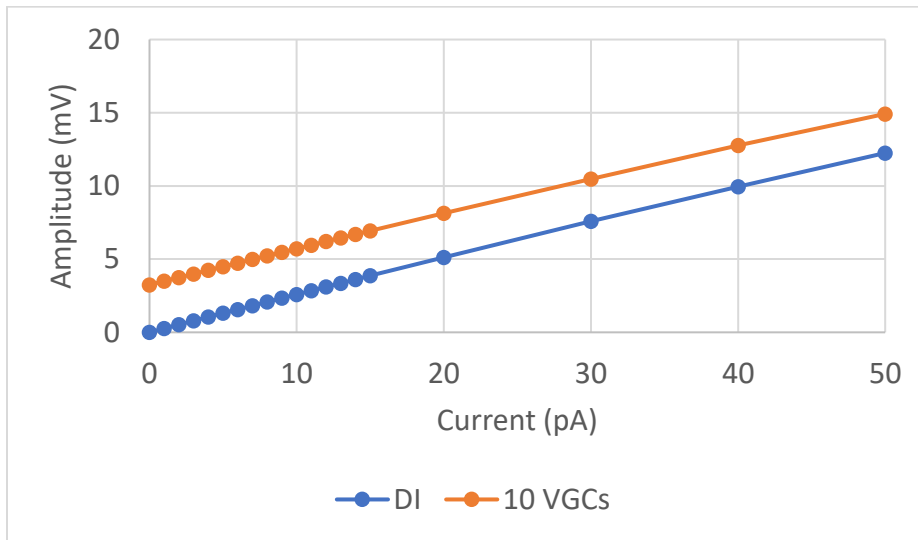

Figure 4.14: Signal amplitude at AIS with only dendritic input, DI, and with only 10 VGCs on the microvilli.

4.2.7 Soma Size

Since a neurons' soma size varies from one neuron to another, the effect of a large soma size on the signal propagation was investigated to see if the presence of somatic VGCs will boost the AIS' amplitude. As described in Section 3.2.1.1, 40 µm x 40 µm cylindrical soma were investigated and compared with the results obtained in Section 4.2.1.

First, the number of segments were investigated to determine how the length of the segment would impact the signal amplitude at the AIS. The segment length of the 40 x 40 soma was varied between 1 µm to 40 µm. The results in Table 4.3 show that there is less than 0.12%, less than 4 µV of a difference in the changes between the smallest one segment and the 40 segments. This is because the space constant, $\lambda = 3.16$ mm, is much bigger than the soma length, $L = 40$ µm. Thus, the signal propagates through the soma will not lose much of its amplitude.

Table 4.3: Comparison between the amplitude changes varying the number of segment of 40 x 40 soma. DI is the dendritic input, AIS is at Axon Initial Segment, and L is the segment length.

segment	L (µm)	Amplitude at AIS		
		DI (mV)	DI+VGC on microvilli (mV)	DI+VGC on soma (mV)
1	40	3.443	3.679	3.684
4	10	3.443	3.683	3.687
10	4	3.443	3.681	3.686
20	2	3.443	3.681	3.686
40	1	3.443	3.683	3.687

Thereafter, VGCs' amplitude was measured for 40 µm x 40 µm soma, 10 segments, and compared with the 10 µm x 10 µm soma. VGCs still boost the AIS signal with a bigger soma size, as shown in Figure 4.15. However, the AIS signal only increased 6.9% with 10 VGCs. In contrast with the smaller soma, the AIS amplitude increased significantly by 89% compared to the dendritic amplitude. Moreover, when the number of channels increased to 40, the AIS amplitude increased

38

26% with a 3.44 input signal, which is very small compared to the 317% increase with 10 µm x 10 µm soma. Therefore, the effect of VGCs decline as the soma size increases, which could indicate that somatic VGCs are only effective in neurons with a small soma, such as ipRGCs.
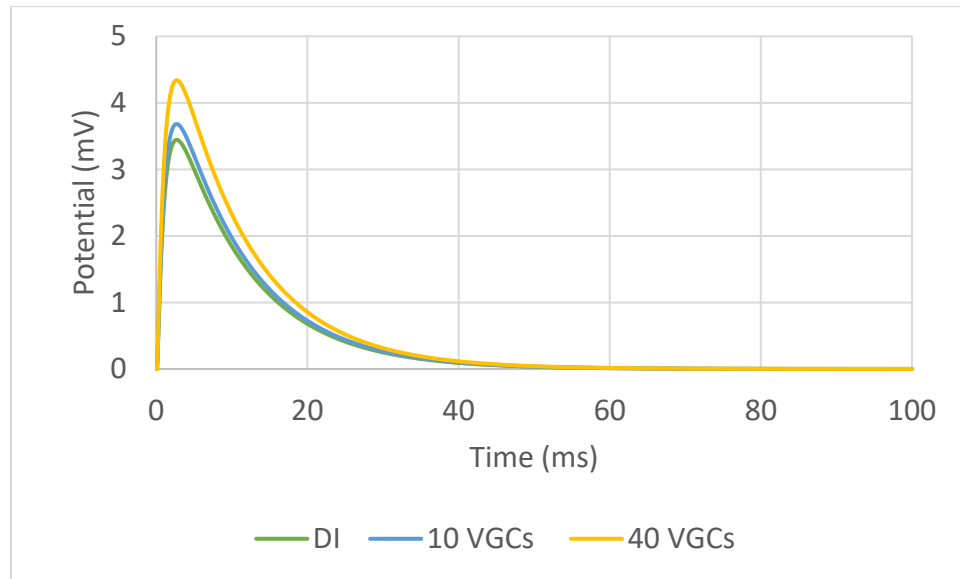
Figure 4.15: Signal amplitude at AIS with only dendritic input, DI, and with only 10 & 40 VGCs on the microvilli attached to 40 µm x 40 µm soma.

4.2.8 Nonlinear Behavior

The results obtained from the circuit model show nonlinear behavior. As seen in Table 4.4, the superposition principle does not apply. The superposition principle states that, in a linear system, the net response of the system is the sum of each stimuli individually [45]. However, when adding the dendritic input signal to the signal coming from the VGCs, the results do not equal the output amplitude obtained when both signals are simulated at the same time. For instance, if the circuit is simulated with 40 VGCs on microvilli, the signal amplitude obtained at AIS is equal 11.488 mV. If the 11.488 mV amplitude obtained from only the VGCs is added to the amplitude obtained at the AIS from 23.23 mV dendritic input, the total algebraic sum of the two stimuli is equal 34.72 mV, which is 3.76 mV higher than the amplitude obtained from simulating the

dendritic input and the VGCs at the same time. This indicates that some aspects of the neuronal electrical behavior could not be accurately investigated using linear circuit model.

Table 4.4: Simulation results with only dendritic input, DI, and only VGCs on microvilli or soma, and both DI and VGCs. The last two columns are the sum of dendritic inputs' amplitude and VGCs' amplitude.

Simulation	Simulation: VGCs signal only (mV)		Simulation: DI & VGCs (mV)		Superposition: DI + VGCs	
DI	Microvilli	Soma	Microvilli	Soma	Microvilli	Soma
3.4394	11.4879	12.3100	14.3631	15.1465	14.9273	15.7494
6.7085	11.4879	12.3100	17.0968	17.8447	18.1964	19.0185
12.7729	11.4879	12.3100	22.1774	22.8542	24.2608	25.0829
23.2328	11.4879	12.3100	30.9524	31.5119	34.7207	35.5428

4.3 Hodgkin-Huxley Model

The results from the HH model in NEURON were obtained and analyzed. The HH model offers the ability to study the electrical behavior of the system by including the nonlinear Na^+ and K^+ gating equations. Therefore, the VGCs will be the voltage triggered and thus, the threshold can be investigated.

In this model, three cases were studied and analyzed: 1) The effect of VGCs position on somatic signal amplitude 2) The threshold values of VGCs with different VGCs densities 3) The input signal coming from microvilli only, without any dendritic input. Each case was simulated two times; once with Na^+ and K^+ VGCs and the other time with only Na^+ VGCs.

4.3.1 Signal Boosting

First, AIS amplitude was measured and analyzed with both Na^+ and K^+ VGCs for different current amount injected. To see how the AIS amplitude is affected by VGCs, the AIS's amplitude

were measured with a passive soma and microvilli, then, VGCs densities were varied from 5 mS/cm^2 Na$^+$ and 1.125 mS/cm^2 K$^+$ to 160 mS/cm^2 Na$^+$ and mS/cm^2 K$^+$. The results of the three cases were studied and analyzed: 1) The presence of VGCs only on soma 2) The presence of VGCs only on microvilli 3) The presence of VGCs in both the soma and microvilli.

4.3.1.1 VGCs on Soma

The presence of VGCs increased the amplitude at AIS. When the injected current resulted in a voltage below the threshold of the VGC, the resulting potential at the AIS increased linearly until it reached its threshold. As seen in Figure 4.16, the curves fall on about the same line below threshold. This linear slope is determined by the membrane capacitance. After the VGCs were triggered, the AIS amplitude will plateau at a certain value based on the VGCs' density as the current injected increases. As the VGCs density increases, the AIS amplitude changes and becomes minimal as the current injected increases. As seen in Table 4.5, even when the current injected at the dendrite doubled, the AIS amplitude does not change significantly, as there is a less than 4% change in amplitude.
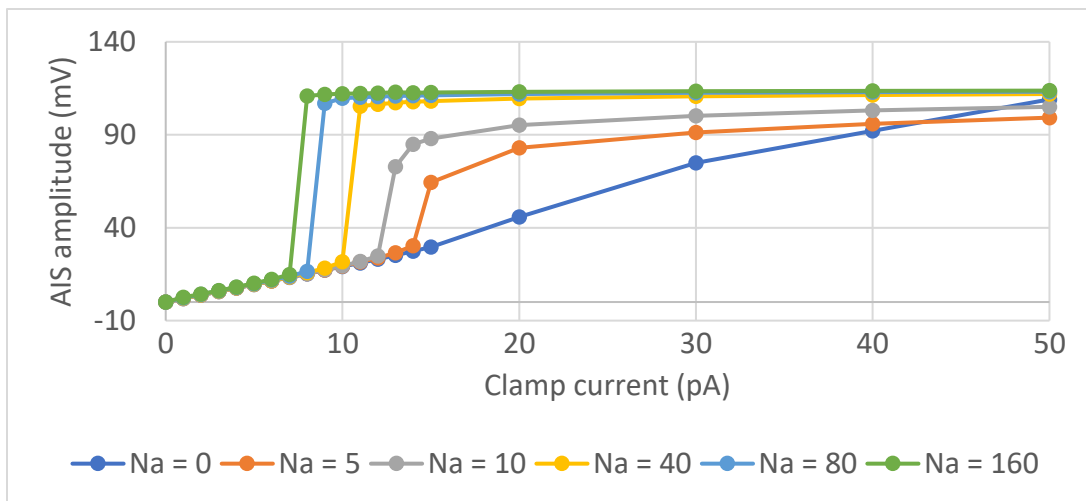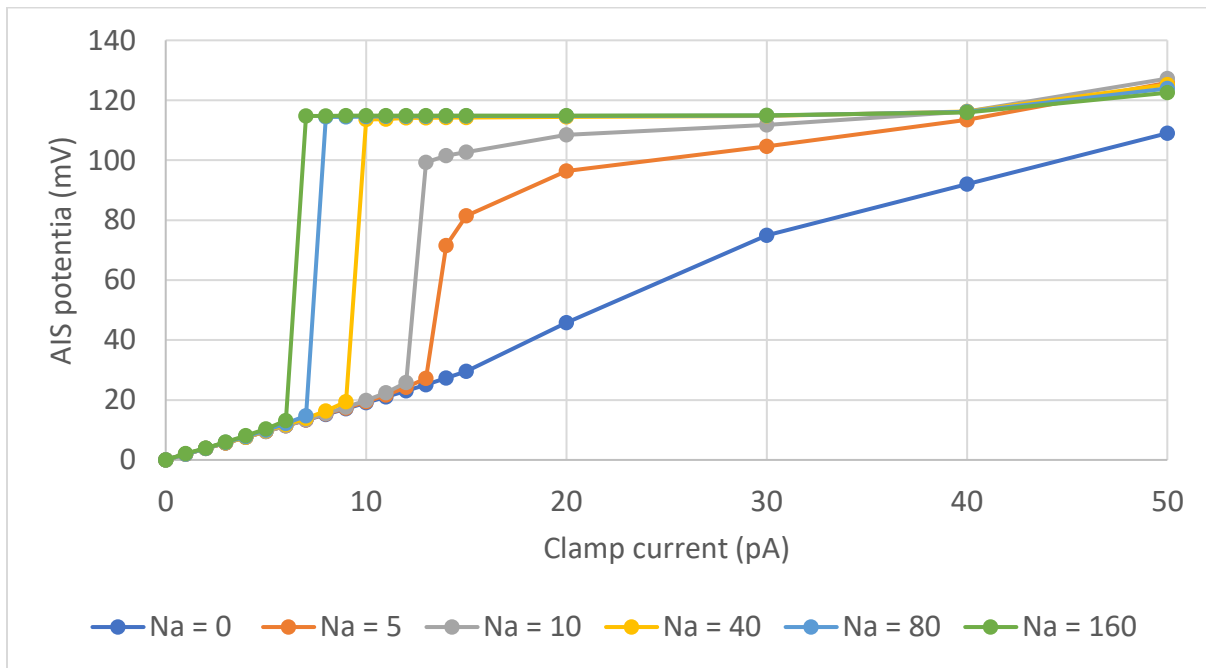

Figure 4.16: Signal amplitude at AIS from the current clamp experiment with different Na$^+$ & K$^+$ VGCs densities (mS/cm^2) on soma. The value presented in the graph is Na$^+$, K$^+$ and is presented on Table 3.5.

Table 4.5: Simulation results from the current clamp experiment with Na⁺ & K⁺ VGCs on soma.

Current (pA)	Amplitude at AIS (mV)					
	No VGCs	Na⁺ = 40 mS/cm²	K⁺ = 9 mS/cm²	Na⁺ = 80 mS/cm²	K⁺ = 18 mS/cm²	Na⁺ = 160 mS/cm²	K⁺ = 36 mS/cm²
0	0	0		0		0	
1	1.8966	2.0366		2.1811		2.4828	
2	3.7926	3.9298		4.0706		4.3615	
3	5.6890	5.8237		5.9609		6.2415	
4	7.5861	7.7219		7.8599		8.1401	
5	9.4845	9.6333		9.7854		10.0984	
6	11.3850	11.5757		11.7771		12.2177	
7	13.2893	13.5863		13.9249		14.7985	
8	15.1998	15.744		16.463		110.8562	
9	17.1207	18.236		106.8965		111.6651	
10	19.0585	21.6315		109.6434		111.9997	
11	21.0235	105.3322		110.2402		112.1996	
12	23.0311	106.4161		110.5720		112.3671	
13	25.1042	107.2892		110.8974		112.9982	
14	27.2762	107.7564		111.0669		112.6104	
15	29.5942	108.1304		111.2490		112.6942	
20	45.8407	109.4230		111.8631		113.0314	
30	74.95185	110.6745		112.5131		113.3860	
40	92.0152	111.4075		112.8862		113.5908	

| 50 | 109.0031 | 111.9224 | 113.1614 | 113.7560 |

Then, the simulation was run for 5 different values of Na^+ VGCs to investigate the effect Na^+ has on the signal amplitude. Higher AIS amplitude values were obtained with the absence of K^+ VGCs (Figure 4.17). Also, the AIS VGCs were triggered faster without K^+ VGCs. However, with the absence of K^+ VGCs, the membrane potential did not return to its steady state potential, as seen in Figure 4.18. Nonetheless, when the model includes both VGCs, the membrane returns to its initial value (Figure 4.19). This is because K^+ VGCs is responsible for repolarizing the membrane [46].Thus, in this model, the presence of somatic K^+ VGCs is crucial to return the membrane potential to its steady state.

Figure 4.17: Signal amplitude at AIS from the current clamp experiment with only Na^+ VGCs on soma.
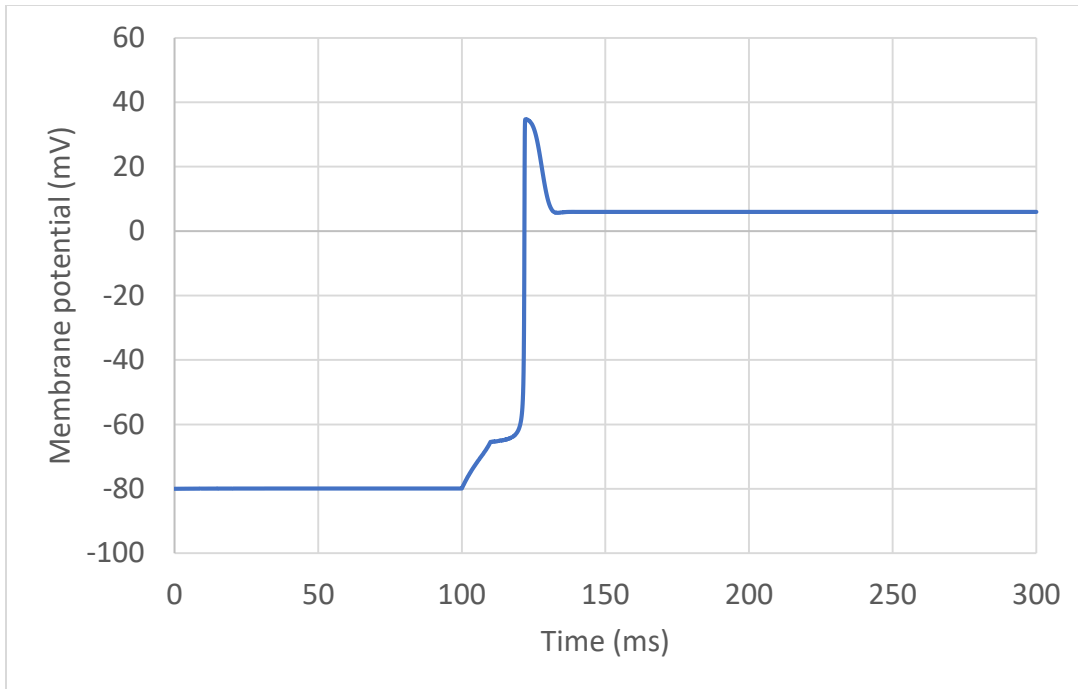
Figure 4.18: Signal amplitude at AIS from the current clamp experiment with only Na$^+$ VGCs, 160 mS/cm^2 on soma.

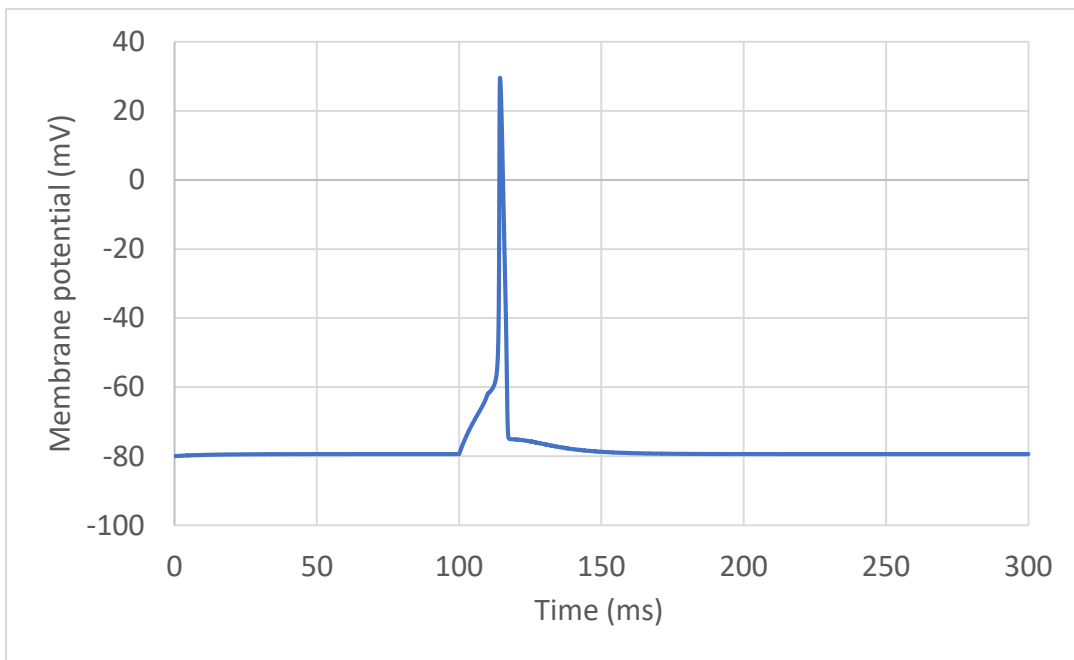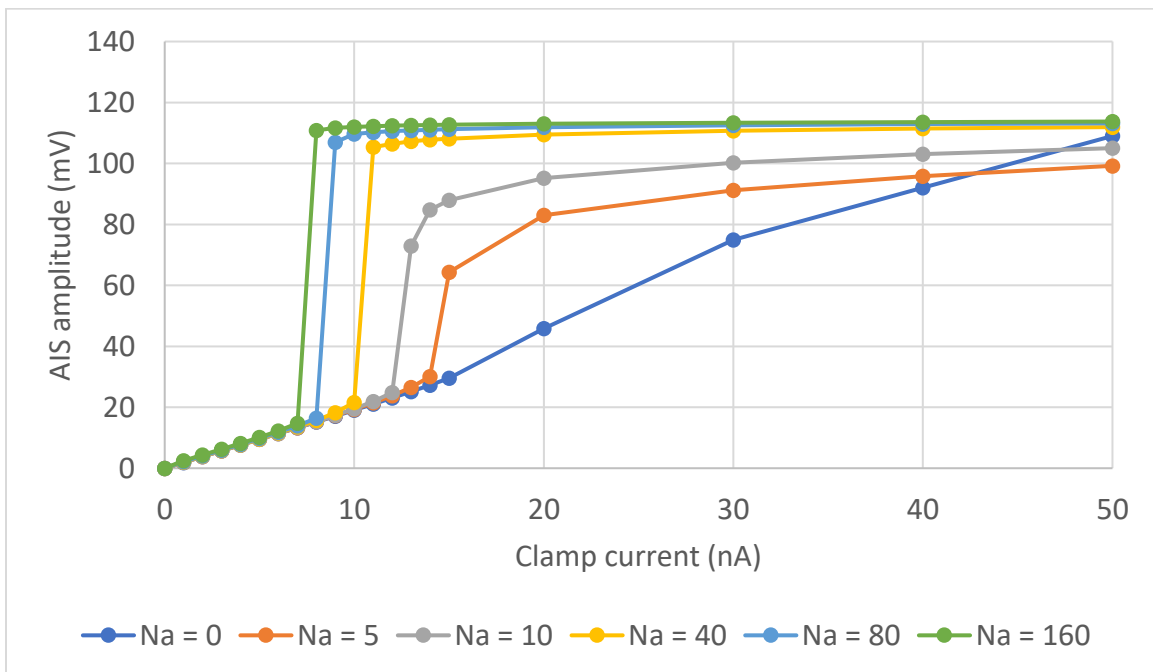**Figure 4.19: Signal amplitude at AIS from the current clamp experiment with Na$^+$ VGCs, 160 mS/cm^2, and K$^+$ VGCs, 36 mS/cm^2 on soma.**

4.3.1.2 VGCs on Soma and Microvilli

Similar results were obtained in this experiment for the result described in the previous section. VGCs increased the AIS's amplitude linearly below VGCs triggering values, as seen in Figure 4.20. There was a small increase in the AIS amplitude with VGCs, in both microvilli and soma, compared to VGCs only on soma. This small increase in AIS amplitude compared to the previous simulation was due to having the VGCs in the microvilli's small area, which will have only a small increase to the AIS's amplitude. This ends up being less than 0.5 mV at most, compared to the VGCs on soma. As a result, inserting VGCs in the microvilli did not lower the current amount required to trigger an action potential at the AIS.

Figure 4.20: Signal amplitude at AIS from the current clamp experiment with different Na$^+$ & K$^+$ VGCs densities on soma & microvilli. The values presented in the graph are Na$^+$, K$^+$ and are presented on Table 3.5.

Excluding K$^+$ VGCs on soma and microvilli have the same effect, as described in the previous section. Without K$^+$ VGCs, the membrane's potential will not return to its resting potential value.

The results obtained from the Hodgkin and Huxley model with VGCs on soma or soma and microvilli show no significant difference in the AIS's amplitude between the two simulations. The two simulation shows same threshold value for the two cases, with and without K$^+$ VGCs. For both simulation after triggering the VGCs, the AIS's amplitude plateaued as the VGCs' density increased. In addition, as seen in Figure 4.21, increasing the VGCs to more than 80 mS/cm^2 does not affect the AIS' amplitude significantly, as there was a less than 1.8% increase.
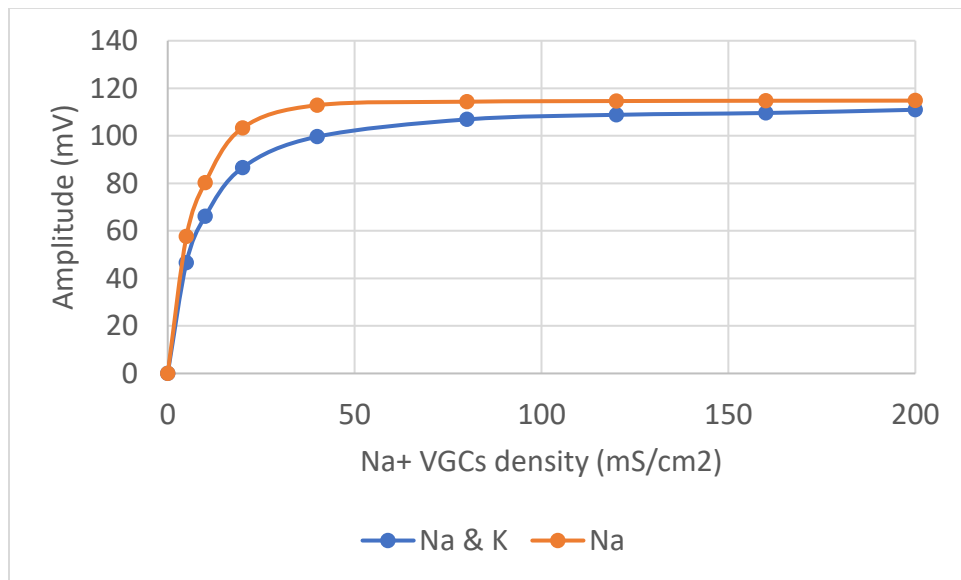
Figure 4.21: AIS amplitude changed compared to Na$^+$ & K$^+$ VGCs densities.

4.3.1.3 VGCs on Microvilli

The AIS' amplitude was measured and analyzed with both Na$^+$ & K$^+$ VGCs for different current amounts injected. To see how the AIS's amplitude is affected by VGCs, the AIS' amplitude was measured without any VGCs on soma and microvilli. Thereafter, the VGCs' density varied from 5 mS/cm^2 Na$^+$ and 1.125 mS/cm^2 K$^+$ to 160 mS/cm^2 Na$^+$ and mS/cm^2 K$^+$. As seen in Figure 4.22, the VGCs' increased the AIS linearly, as the current injected at the dendrite increased. The increase in the AIS' amplitude, however, only had a slight change, 2% increase at most, when 20 pA was injected. After that, the AIS' amplitude slightly declined as the current amount increased.

Notably, as seen in Figure 4.23, as the VGCs' density increased, the AIS's amplitude declined more steeply after the VGCs were triggered to a value less than the results from the model without any VGCs. This shows that K^+ VGCs dominated the VGCs' signal on the microvilli, even though it has low density compared to Na^+ VGCs.
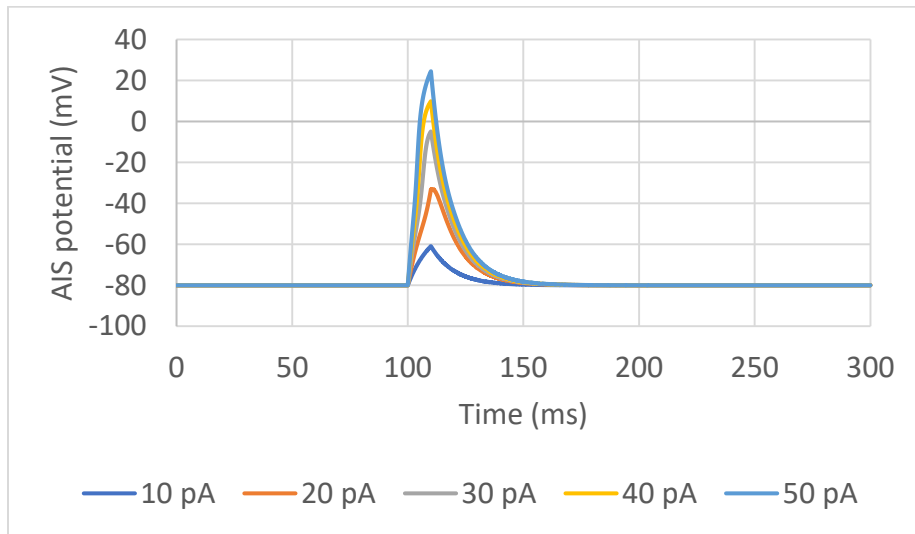
Figure 4.22: Signal amplitude at AIS from the current clamp experiment with Na^+ VGCs 160 mS/cm^2 & K^+ VGCs 36 mS/cm^2 on microvilli from the current clamp experiment.
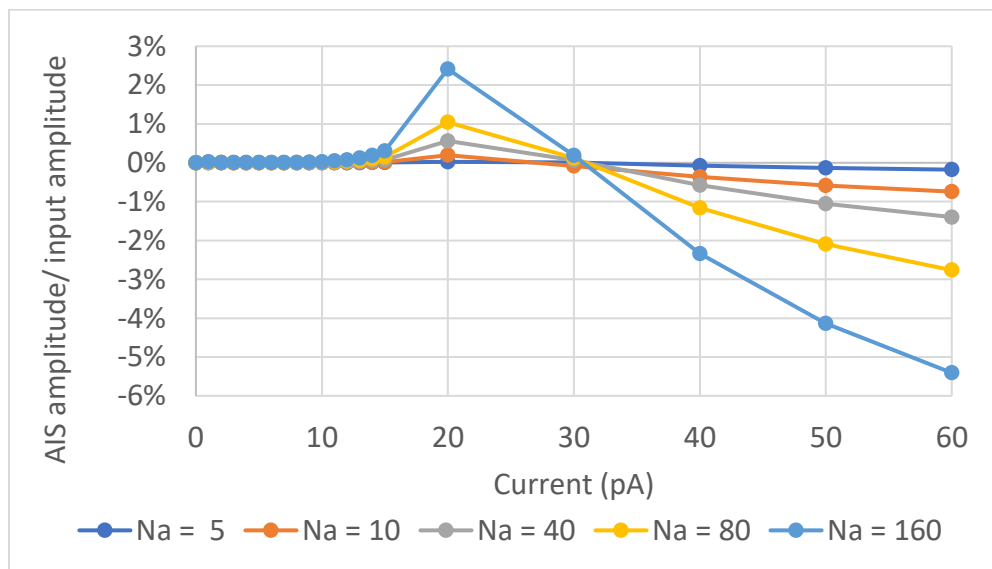
Figure 4.23: Percentage of AIS' amplitude that changed compared to the dendritic input with Na^+ & K^+ VGCs on microvilli.

Second, the K$^+$ VGCs was excluded from the model. Na$^+$ VGCs' density was varied, as described in the method. To cover a wider range, Na$^+$ VGCs' density was increased up to 5 times the number reported for retinal ganglion cells [39], [47]. Table 4.6 present the results of this model. The AIS' amplitude had a marginal change as the density increased. The highest changes happened around the triggering of Na$^+$ VGCs, - 34 mV, with a less than 9% increase compared to the amplitude with no VGCs. However, omitting K$^+$ VGCs made the AIS' amplitude slightly increase as the density increased (Figure 4.24). In addition, the membrane potential returned to its resting potential after removing the stimuli at the dendrite, even without K$^+$ VGCs, which indicates that the presence of VGCs on microvilli have a minimal effect on the somatic signal propagation.

Table 4.6: Simulation results from the current clamp experiment with different microvilli Na$^+$ VGCs densities

Current (pA)	Amplitude at AIS at different Na$^+$ VGCs densities (mV)							
	0 mS/cm²	5 mS/cm²	40 mS/cm²	80 mS/cm²	160 mS/cm²	240 mS/cm²	320 mS/cm²	400 mS/cm²
0	0	0	0	0	0	-	-	-
1	1.896	1.896	1.896	1.896	1.896	-	-	-
2	3.792	3.792	3.792	3.792	3.792	-	-	-
3	5.689	5.689	5.689	5.689	5.689	-	-	-
4	7.586	7.586	7.586	7.586	7.586	-	-	-
5	9.484	9.484	9.484	9.484	9.485	-	-	-
6	11.385	11.385	11.385	11.385	11.386	-	-	-
7	13.289	13.289	13.289	13.290	13.291	-	-	-
8	15.199	15.199	15.200	15.201	15.202	-	-	-

9	17.120	17.120	17.122	17.123	17.126	-	-	-
10	19.058	19.058	19.060	19.063	19.067	19.072	19.076	19.081
20	45.840	45.913	46.181	46.482	46.925	47.816	48.804	49.658
30	74.951	75.304	75.304	75.654	76.347	77.029	77.701	78.361
40	92.015	92.300	92.300	92.582	93.139	93.684	94.220	94.744
50	109.003	109.033	109.243	109.481	109.950	110.408	110.856	111.294
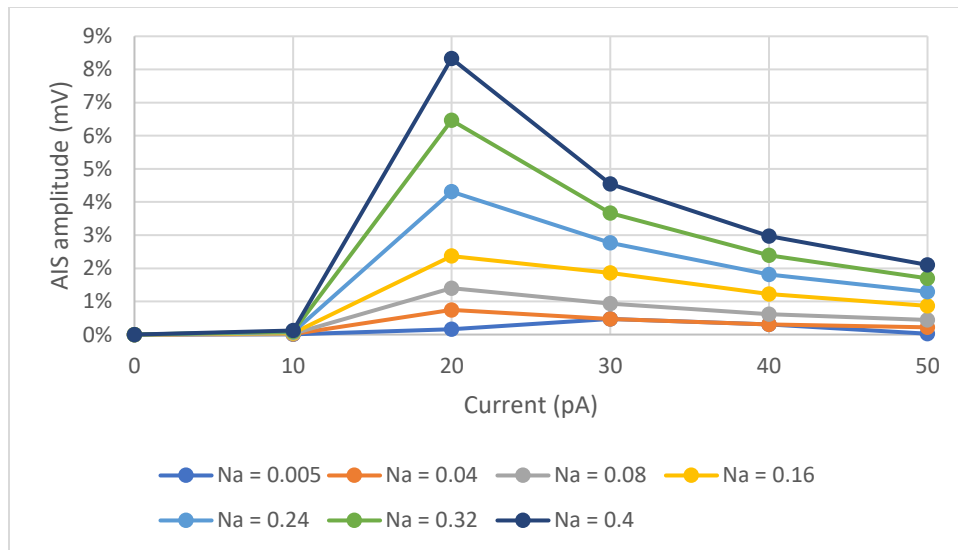
Figure 4.24: Percentage of AIS' amplitude changed compared to the dendritic input with Na$^+$ VGCs only on microvilli.

Moreover, the number of microvilli increased to two and four microvilli to investigate how it effects somatic signal propagation. The results obtained from the two and four microvilli show similar observations to the one microvilli results (Figure 4.25 and 4.26). With both Na+ and K+ VGCs included in the model, the AIS' amplitude declined more steeply after the VGCs triggered and the number of microvilli increased. However, on the other hand, without K+ VGCs, the AIS's

amplitude slightly increased as the number of microvilli increased. In conclusion, increasing the number of microvilli had an insignificant effect on the AIS' amplitude.
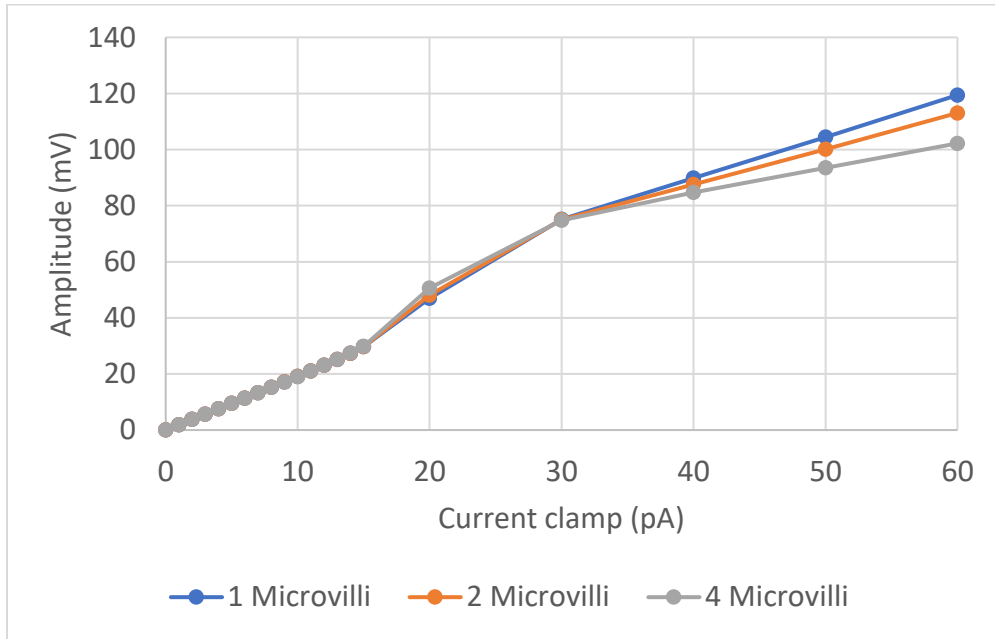

Figure 4.25: AIS amplitude with 160 mS/cm^2 Na$^+$ & 36 mS/cm^2 K$^+$ VGCs on 1,2, and 4 microvilli.
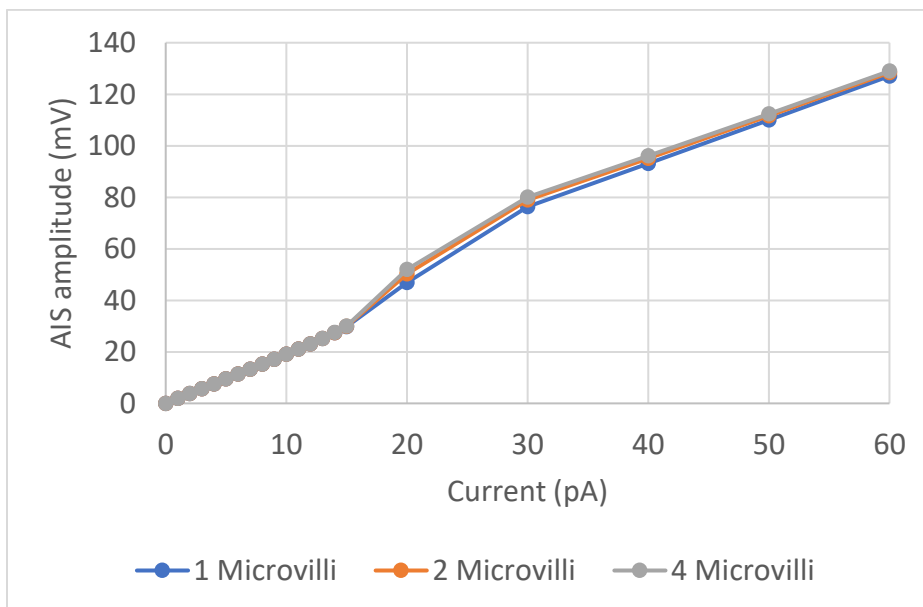

Figure 4.26: AIS amplitude with 160 mS/cm^2 Na$^+$ VGCs on 1,2, and 4 microvilli.

4.3.2 VGCs Threshold

The threshold values were measured for each VGCs' density value. To find the threshold value associated with each VGCs' densities, the current injected into the dendrite was incremented by 0.1 pA until the action potential is initiated at the AIS. As expected, the threshold lowered as the VGCs' density increased, as shown in Table 4.7.

Table 4.7: Threshold values for different VGCs' densities on soma

VGCs density (mS/cm^2)		VGCs on Soma (mV)	
Na$^+$	K$^+$	Na$^+$ & K$^+$	Only Na$^+$
5	1.125	37.102	31.220
10	2.25	31.027	25.782
40	9	22.644	19.819
80	18	20.426	16.924
160	36	17.485	14.560
200	45	19.010	13.484
240	54	18.635	12.384
320	72	16.410	11.882

4.3.3 Microvilli Signal

The expression of Na$^+$ VGCs in ipRGCs soma, as seen in Figure 2.3, might indicate that these cells could receive input signals directly from VGCs on somatic microvilli. Thus, in this simulation, the current is injected at the microvilli to see how the signal propagates to the AIS. The simulation was run three times, without any VGCs, with Na$^+$ & K$^+$ VGCs, and with only Na$^+$ VGCs. Results are presented on Table 4.8.

Table 4.8: AIS & microvilli signals' amplitude with the current injected to the microvilli

Current (pA)	No VGCs (mV)		Na$^+$ & K$^+$ VGCs (mV)		Na$^+$ VGCs (mV)	
	Microvilli	AIS	Microvilli	AIS	Microvilli	AIS
1	2.07	1.90	2.07	1.90	2.07	1.90
2	4.14	3.79	4.14	3.79	4.14	3.79
3	6.21	5.69	6.21	5.69	6.21	5.69
4	8.28	7.59	8.28	7.59	8.28	7.59
5	10.35	9.48	10.35	9.48	10.35	9.48
6	12.43	11.38	12.43	11.38	12.43	11.38
7	14.51	13.29	14.51	13.29	14.51	13.29
8	16.59	15.20	16.59	15.20	16.59	15.20
9	18.69	17.12	18.69	17.12	18.69	17.12
10	20.80	19.06	20.80	19.06	20.80	19.06
11	22.94	21.02	22.94	21.03	22.95	21.03
12	25.12	23.03	25.13	23.04	25.14	23.05
13	27.36	25.10	27.39	25.12	27.40	25.13
14	29.71	27.28	29.75	27.31	29.77	27.32
15	32.20	29.59	32.28	29.66	32.30	29.67
20	49.36	45.89	49.94	46.43	50.06	46.53
30	80.17	74.95	80.05	74.89	80.87	75.64
40	98.97	92.01	97.31	90.63	99.51	92.55
50	117.70	109.00	114.59	106.28	118.15	109.45

As seen in Table 4.6, when the signal was propagated from the microvilli to the AIS, the signal's amplitude decreased. The signal lost less than 8.5% of its amplitude due to the high microvilli neck resistance. This indicates that the microvilli neck resistance acts as an electric compartment that reduces the signal injected into the cell [15]. On the other hand, injecting a current to the microvilli did not initiate an action potential in the AIS, as the current injected increased (Figure 4.27). Moreover, there was no significant change when the VGCs are included, as there was a less than 0.2% change.
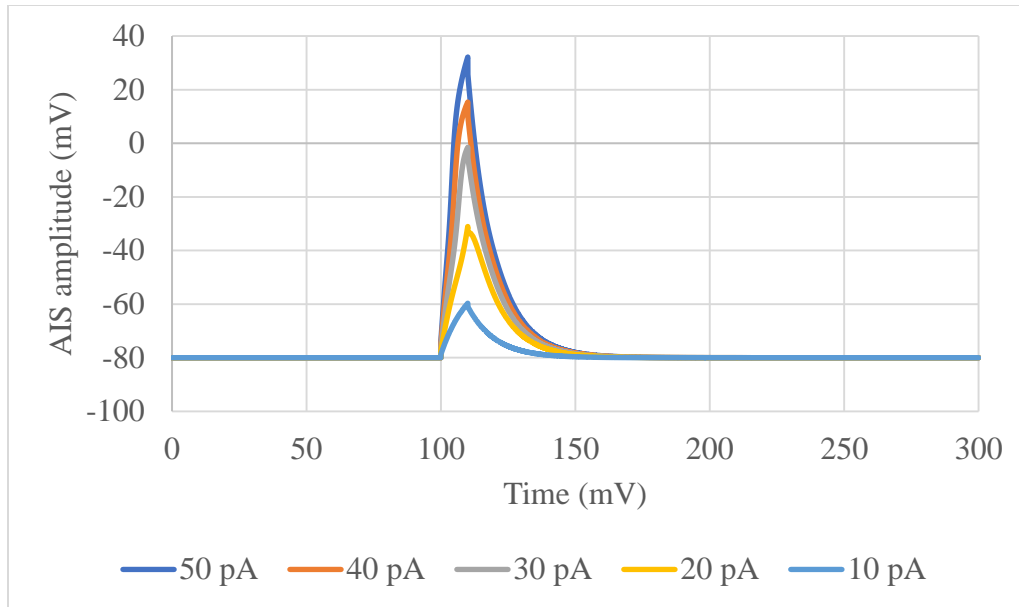
Figure 4.27: AIS' amplitude with 80 mS/cm^2 Na$^+$ VGCs & 80 mS/cm^2 K$^+$ VGCs for different current amount.

Finally, compared to the Hodgkin-Huxley model and the circuit model, both models show similar results below the VGCs' threshold. In the Hodgkin-Huxley model, the AIS' amplitude increased linearly, as the dendritic input increased below the VGCs' triggering value, which indicated that the model behaves as a passive model below the threshold. On the other hand, in the circuit model, the VGCs are time triggers, which means that the AIS's amplitude is always affected by both the dendritic input and the VGCs' signals. While on the Hodgkin-Huxley model, the ion channels are voltage-dependent, which indicates that the effect of these VGCs will not be seen unless the threshold value is reached. Thus, the Hodgkin-Huxley model is more realistic than the circuit model.

CHAPTER 5: CONCLUSIONS

In conclusion, this thesis presents, to the author's knowledge, the first research on electrical behavior of VGCs on somatic microvilli. The overall objective of this MS was to study the effect of VGCs on microvilli on somatic signals and design models to investigate the microvilli's electrical behavior.

5.1 Conclusions Remarks

In this section, concluding remarks for each model are given.

5.1.1 Circuit Model

The ipRGCs soma and microvilli were modeled and studied using a MATLAB Simulink circuit model. The study was extended to obtain the difference in AIS's voltage amplitude by varying the VGCs' position between the soma shaft and microvilli. The AIS' amplitude had an insignificant difference between the two positions. However, as the VGCs' density increased from 10 channels to 40 channels, the position of the VGCs became more significant as the AIS's amplitude was reduced when the VGCs were located on microvilli compared to the soma. This decline of the AIS's amplitude was resulted by the microvilli neck resistance attenuates the VGCs' signal as the signal propagate to the AIS. Moreover, increasing the neck resistance will reduce the microvilli' VGCs amplitude further. This could imply that the microvilli play an important role in reducing the probability of the VGCs misfiring.

Moreover, the study demonstrates how the soma size impacted the somatic signal's amplitude. The effect of VGCs decreased as the soma size increased. When the soma size

quadrupled, the AIS's amplitude declined 13 folds. Thus, somatic VGCs might only be expressed in neurons with small sizes, such as ipRGCs.

5.1.2 Hodgkin-Huxley Model

The somatic VGCs were modeled and studied using the Hodgkin and Huxley model. initially, Na^+ and K^+ VGCs were positioned only on the soma. The results show that below the VGCs' threshold, the model linearly increased the AIS's amplitude as the injected current from clamp increased. Also, below the threshold, the AIS exhibits no change in amplitude, while the Na^+ and K^+ VGCs' densities increased. On the other hand, increasing the Na^+ VGCs' density lowered the threshold, as expected. Thereafter, Na^+ and K^+ VGCs were positioned on the soma and microvilli. The results show no significant difference when the VGCs were positioned on both the microvilli and the soma compared to positioning VGCs only on the soma. The highest difference in the results from the two simulations was less than 0.2%, which was expected since the number of microvilli's VGCs is very small compared to the number of soma's VGCs.

Moreover, as seen from the results obtained from the previous two simulations, omitting K^+ VGCs reduced the threshold values further. However, without K^+ VGCs, the membrane's potential will not return to its steady state value. Thus, including K^+ VGCs in the model is crucial to having a reliable neuron model.

next, the simulation was run with Na^+ and K^+ VGCs only placed on the microvilli. The results showed a linear relationship between the current injected and the AIS' amplitude. The highest increase was about 7%, which took place when the Na^+ VGCs' density was multiplied 5 times higher than the reported value for Na^+ VGCs in retinal ganglion cells. Thereafter, we tested the hypothesis, which questioned if the microvilli Na^+ VGCs could receive input signals. The results obtained from the simulation showed that the model behaved as a passive model. However,

the signal's amplitude was reduced as it propagated to the AIS because of the high neck resistance, which acts as an electrical compartment that attenuated the signal.

5.2 Future Work

In regard to the circuit model, a voltage-dependent variable resistor that represents VGCs will result in more accurate results for the somatic signals. Modeling a VGCs as voltage-dependent variable resistor allows the inclusion of the effect of other VGCs, such as K^+ and Cl^-, to have more accurate representations of the factors that influence the electrical signal's behavior in neurons. In addition, the model can improve the nonlinear behavior of the model above its threshold. For example, by making voltage-dependent variable resistors triggered on certain threshold potentials.

For a better understanding of the presence of VGCs on somatic microvilli, the development of a model based on the Poisson- Nernst-Plank (PNP) equation of electrodiffusion might be necessary. Both models used in this research are based on the assumption that there is no interaction between the electric and diffusive flux. Such an assumption can be made for small neuronal compartments [48], [49]. Therefore, a model based on the PNP equation, where both diffusive and the electrical flux is accounted for, could improve the accuracy and the reality of the results.

REFERENCES

[1]   L. Beaulieu-Laroche and M. T. Harnett, "Dendritic Spines Prevent Synaptic Voltage Clamp," *Neuron*, vol. 97, no. 1, p. 75–82.e3, 2017.

[2]   Private conection with Jozsef Vigh ,Colorado State University,"No Title," 2018.

[3]   J. DeFelipe, "The dendritic spine story: an intriguing process of discovery," *Front. Neuroanat.*, 2015.

[4]   R. Yuste, "The discovery of dendritic spines by Cajal," *Front. Neuroanat.*, vol. 9, no. April, pp. 1–6, 2015.

[5]   E. D. P. DeRobertis and H. Stanley Bennett, "SOME FEATURES OF T H E SUBMICROSCOPIC MORPHOLOGY OF SYNAPSES IN FROG AND EARTHWORM*," 1954.

[6]   E. G. Gray, "Electron microscopy of synaptic contacts on dendrite spines of the cerebral cortex," *Nature*, vol. 183, no. 4675, pp. 1592–1593, 1959.

[7]   R. Yuste, "Dendritic Spines and Distributed Circuits," *Neuron*, vol. 71, pp. 772–781, 2011.

[8]   D. B. Chklovski, "Synaptic Connectivity and Neuronal Morphology: Two Sides of the Same Coin," *Neuron*, vol. 43, pp. 609–617, 2004.

[9]   Q. Wen, A. Stepanyants, G. N. Elston, A. Y. Grosberg, D. B. Chklovskii, and C. F. Stevens, "Maximization of the connectivity repertoire as a statistical principle governing the shapes of dendritic arbors," 2009.

[10]   S. Konur and R. Yuste, "Imaging the motility of dendritic protrusions and axon terminals: roles in axon sampling and synaptic competition," *Mol. Cell. Neurosci.*, vol. 27, no. 4, pp. 427–440, Dec. 2004.

[11]   A. T. Gulledge, N. T. Carnevale, and G. J. Stuart, "Electrical advantages of dendritic spines," *PLoS One*, vol. 7, no. 4, 2012.

[12]   C. D. Acker, E. Hoyos, and L. M. Loew, "EPSPs Measured in Proximal Dendritic Spines of Cortical Pyramidal Neurons," *eNeuro*, vol. 3, no. 2, pp. 50–15, 2016.

[13]   J. Cartailler, T. Kwon, R. Yuste, and D. Holcman, "Deconvolution of Voltage Sensor Time Series and Electro-diffusion Modeling Reveal the Role of Spine Geometry in Controlling Synaptic Strength," *Neuron*, Feb. 2018.

[14]   T. M. H. Trong, S. E. Motley, J. Wagner, R. R. Kerr, and J. Kozloski, "Dendritic spines modify action potential back-propagation in a multicompartment neuronal model," vol. 61, no. 2, pp. 1–13, 2017.

[15]   T. Kwon *et al.*, "Attenuation of Synaptic Potentials in Dendritic Spines," *CellReports*, vol. 20, no. 5, pp. 1100–1110, 2017.

[16]   K. Jayant *et al.*, "Targeted intracellular voltage recordings from dendritic spines using quantum-dot-coated nanopipettes," 2016.

[17]   L. M. Palmer and G. J. Stuart, "Membrane Potential Changes in Dendritic Spines during Action Potentials and Synaptic Input," *J. Neurosci.*, 2009.

[18]   C. Koch ' and A. Zador, "The Function of Dendritic Spines: Devices Subserving Biochemical Rather Than Electrical Compartmentalization," *J. Neurosci.*, vol. 13, no. 2,

1993.

[19]   M. A. Popovic, N. Carnevale, B. Rozsa, and D. Zecevic, "Electrical behaviour of dendritic spines as revealed by voltage imaging," *Nat. Commun.*, 2015.

[20]   -A. Elaagouby and R. Yuste, "Role of Calcium Electrogenesis in Apical Dendrites: Generation of Intrinsic Oscillations by an Axial Current," *J. Comput. Neurosci.*, vol. 7, pp. 41–53, 1999.

[21]   W. R. Holmes, "Is the function of dendritic spines to concentrate calcium?," *Brain Res.*, vol. 519, no. 1–2, pp. 338–342, Jun. 1990.

[22]   F. Faraci, S. Hille, and M. Timme, "The 60th anniversary of the Hodgkin-Huxley model : a critical assessment from a historical and modeller ' s viewpoint," 2013.

[23]   L. Lapicque, "Quantitative investigations of electrical nerve excitation treated as polarization."

[24]   L. F. Abbott, "Lapicque's introduction of the integrate-and-fire model neuron (1907)," 1999.

[25]   W. Teka, T. M. Marinov, and F. Santamaria, "Neuronal Spike Timing Adaptation Described with a Fractional Leaky Integrate-and-Fire Model," *PLOS Comput. Biol.*, vol. 10, no. 3, p. e1003526, Mar. 2014.

[26]   A. L. Hodgkin and A. F. Huxley, "A QUANTITATIVE DESCRIPTION OF MEMBRANE CURRENT AND ITS APPLICATION TO CONDUCTION AND EXCITATION IN NERVE," *J. Physiol. I*, vol. 7, pp. 500–544, 1952.

[27]   P. Nelson, *Biological Physics.* .

[28]   W. Rall, "Core Conductor Theory and Cable Properties of Neurons," *Compr. Physiol.*, 1977.

[29]   S. Hattar *et al.*, "Melanopsin and rod–cone photoreceptive systems account for all major accessory visual functions in mice."

[30]   D. Cao and P. A. Barrionuevo, "The importance of intrinsically photosensitive retinal ganglion cells and implications for lighting design," 2011.

[31]   "Simulink® User's Guide," 2018.

[32]   P. Author, M. E. Larkum, T. Nevian, M. Sandler, A. Polsky, and J. Schiller, "Synaptic Integration in Tuft Dendrites of Layer 5 Pyramidal Neurons: A New Unifying," *Source Sci. New Ser. Biochim. Biophys. Acta Proc. Nati Acad. Sei. U.S.A. J. Silhavy*, vol. 325, no. 191, pp. 756–760, 2009.

[33]   W. R. Holmes, "Space (Length) Constant, Lambda, in Neuronal Signaling," in *Encyclopedia of Computational Neuroscience*, D. Jaeger and R. Jung, Eds. New York, NY: Springer New York, 2013, pp. 1–2.

[34]   M. T. Harnett, J. K. Makara, N. Spruston, W. L. Kath, and J. C. Magee, "Synaptic amplification by dendritic spines enhances input cooperativity," *Nature*, vol. 491, no. 7425, pp. 599–602, 2012.

[35]   R. Araya, R. Benavides-Piccione, and C. Portera-Cailliau, "Input transformation by dendritic spines of pyramidal neurons," 2014.

[36]   F. Contl, B. Hillet, B. Neumoke, W. Nonnert, and R. Stampfli, "MEASUREMENT OF THE CONDUCTANCE OF THE SODIUM CHANNEL FROM CURRENT

FLUCTUATIONS AT THE NODE OF RANVIER t Recipient of an award from the Alexander von Humboldt Foundation, Bonn-Bad Godesberg, Federal Republic of Germany and on leave from," vol. 262, pp. 699–727, 1976.

[37] Z. F. Mainen, J. Joerges, J. R. Huguenard, and T. J. Sejnowski ', "A Model of Spike Initiation in Neocortical Pyramidal Neurons," *Neuron*, vol. 15, pp. 1427–1439, 1995.

[38] T. Vora, B. Corry, and S.-H. Chung, "A model of sodium channels," 2004.

[39] B. W. Sheasby and J. F. Fohlmeister, "Impulse Encoding Across the Dendritic Morphologies of Retinal Ganglion Cells," *Am. Physiol. Soc.*, 1999.

[40] N. T. Carnevale and M. L. Hines, *The NEURON book*. Cambridge University Press, 2006.

[41] T. Kwon, M. Sakamoto, D. S. Peterka, and R. Yuste, "Attenuation of Synaptic Potentials i n Dendritic Spines," *Cell Rep.*, vol. 20, no. 5, pp. 1100–1110, 2017.

[42] R. Araya, J. Jiang, K. B. Eisenthal, and R. Yuste, "The spine neck filters membrane potentials," 2006.

[43] *The Computing Dendrite*. 2014.

[44] R. C. Cannon, C. O 'donnell, M. F. Nolan, and L. J. Graham, "Stochastic Ion Channel Gating in Dendritic Neurons: Morphology Dependence and Probabilistic Synaptic Activation of Dendritic Spikes," *PLoS Comput Biol*, vol. 6, no. 8, 2010.

[45] R. G. Holmes, *Superposition theorem*. Litton Instructional Materials, 1966.

[46] A. F. Huxley, "Hodgkin and the action potential 1935–1952," *1935-1952*.

[47] J. F. Fohlmeister and R. F. Miller, "Impulse Encoding Mechanisms of Ganglion Cells in

the Tiger Salamander Retina," 1997.

[48]   L. P. Savtchenko, M. M. Poo, and D. A. Rusakov, "Electrodiffusion phenomena in
       neuroscience: A neglected companion," *Nat. Rev. Neurosci.*, vol. 18, no. 10, pp. 598–612,
       2017.

[49]   D. Holcman and R. Yuste, "The new nanophysiology: regulation of ionic flow in neuronal
       subcompartments," *Nat. Rev. Neurosci.*, vol. 16, no. 11, pp. 685–692, 2015.

[50]   "A NEURON Programming Tutorial - Part A." [Online]. Available:
       http://web.mit.edu/neuron_v7.4/nrntuthtml/tutorial/tutA.html. [Accessed: 14-Jun-2018].

APPENDIX A: CIRCUIT MODEL

A.1 Signal Boosting

The output signal at the AIS at different VGC's conductance with 3.44 mV, 6.71, 12.77 mV, and 23.23 mV dendritic input.
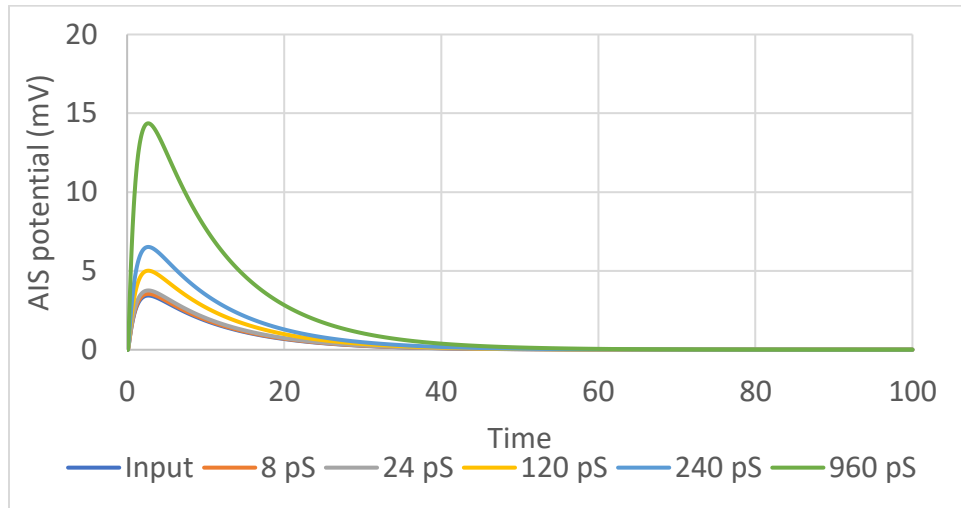
Figure A.1: Output signal at AIS with 3.44 mV input and different VGCs conductance
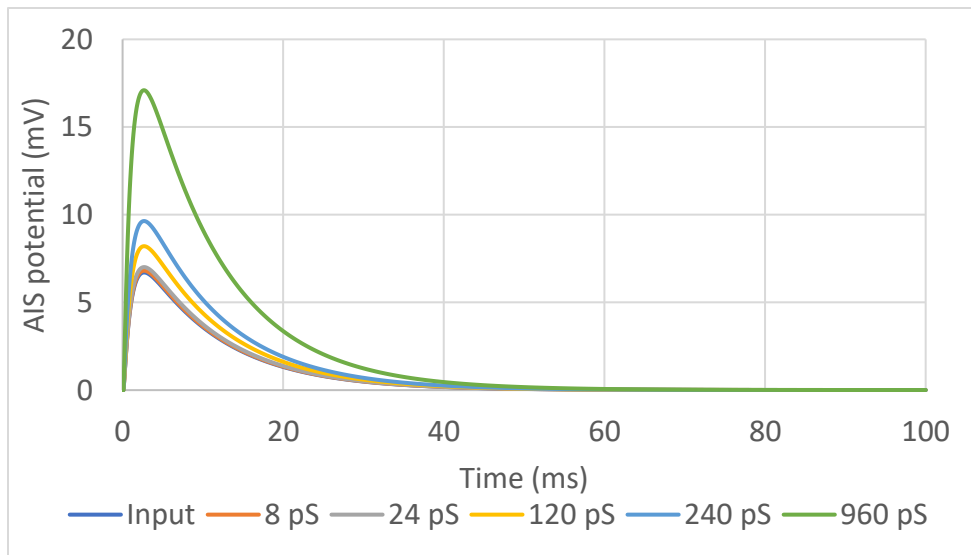
Figure A.2: Output signal at AIS with 6.71 mV input and different VGCs conductance
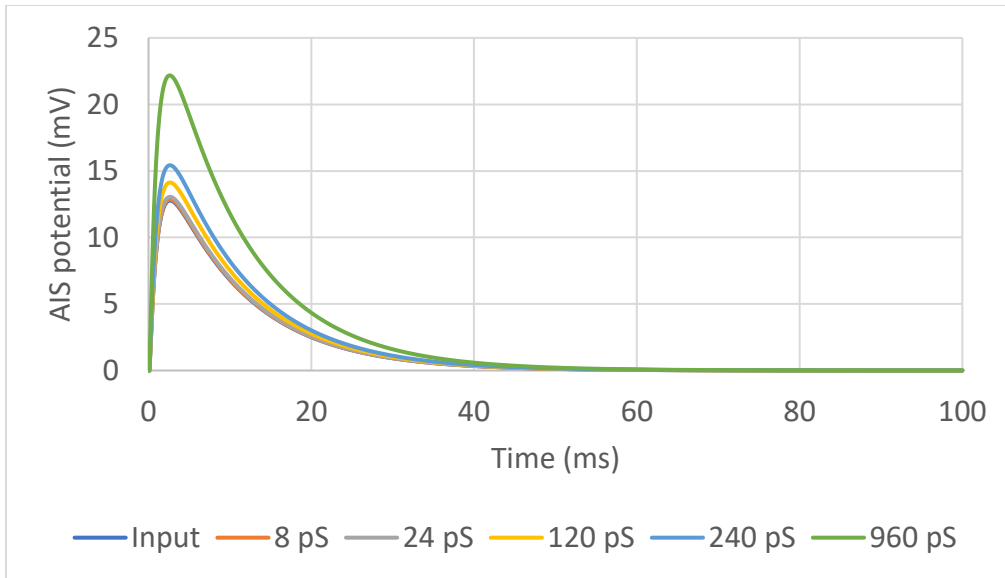
Figure A.3: Output signal at AIS with 12.77 mV input and different VGCs conductance.
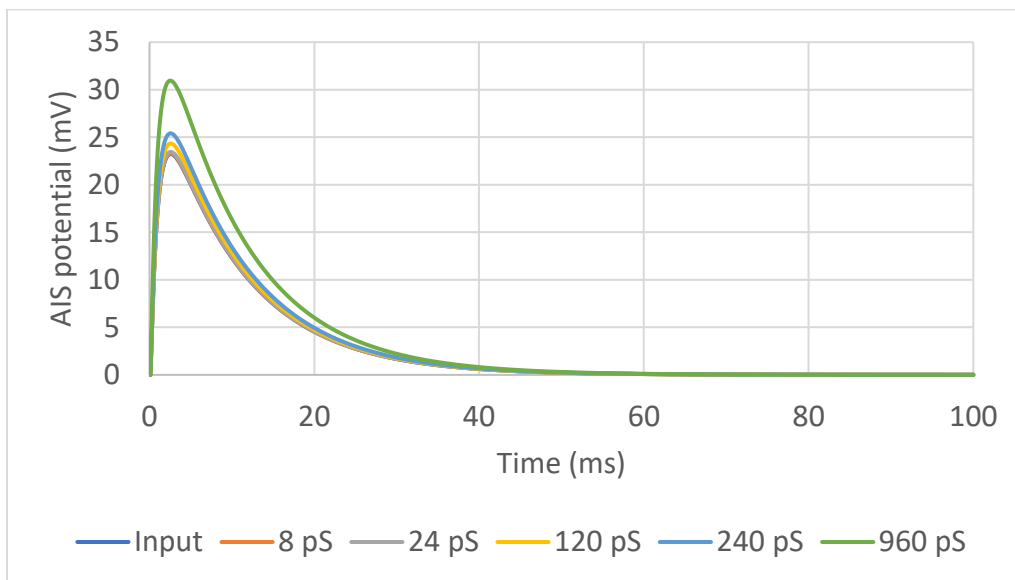
Figure A.3: Output signal at AIS with 23.23 mV input and different VGCs conductance.

A.2 Misfiring Experiment

This is an example overall diagram of the Simulink circuit used to investigate the effect of microvilli misfiring. The circuit contains three blocks, a dendritic input block, a soma block, and an AIS block.

1) Dendritic Input Block:

- A variable time-dependent resistor was inserted to generate the dendritic input signal.

- A Simulink-PS Converter was inserted and connected it to the PS terminal of the variable resistor. PS stands for physical signal. In Simulink, a Simulink-PS Converter block is necessary to the input signal from the MATLAB function block into a physical signal used in the circuit.

- A MATLAB function block was inserted and connected to the S terminal of the Simulink-PS Converter block. The MATLAB function was used to control the conductance of the variable resistor by coding Eq 3.1. The code used in this block is:

```
function R = Synapse(t)
gmax = 2e-9;
gleak = 1e-14;
taur = 0.0001;
tauf = 0.001;
R=1/(gleak+gmax*(exp(-t/tauf)-exp(-t/taur))/1.03);
end
```

- A Repeating Sequence Interpolated box was inserted and connected to the MATLAB function block. This box was used to create a periodic discrete-time sequence which was used as an input to MATLAB function block. Figure A.5 shows the dendritic input block.
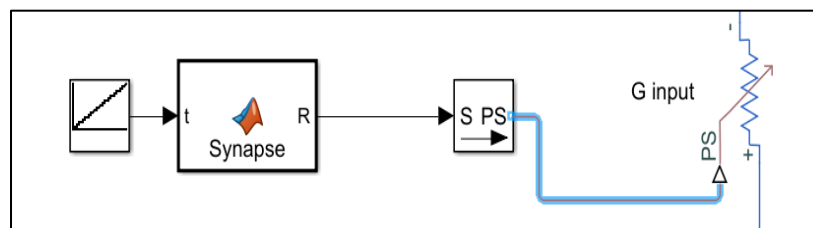
Figure A.5: Dendritic input signal block.

2) Soma Block:

The soma block consists of 10 soma segments and 2 microvilli segments. All soma segments were identical. The following steps were used to build one somatic segment:

- Three resistors, a capacitor, and a DC voltage source were inserted and connected together to form one segment of the soma model as shown in Figure A.6.
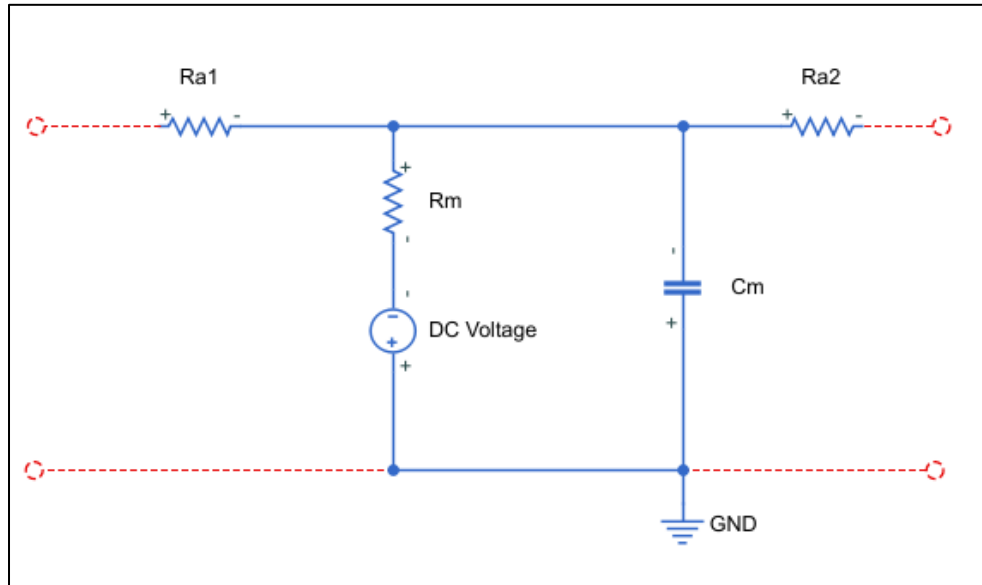
Figure A.6: Single somatic segment.

- Connect this segment to 9 more identical segments and connect them together.

- Then, two microvilli segments were created that are similar to somatic segments, but with different values (Table 3.3). Each microvilli segment was connected to one soma segment by the microvilli axial resistor, R_{neck}.

- Finally, a VGCs block was created following the same steps used in the dendritic input block. Then, the VGCs block was connected in parallel with one of the microvilli segments as seen in Figure A.7, and this circuit is connected to a soma segment through a neck resistance.
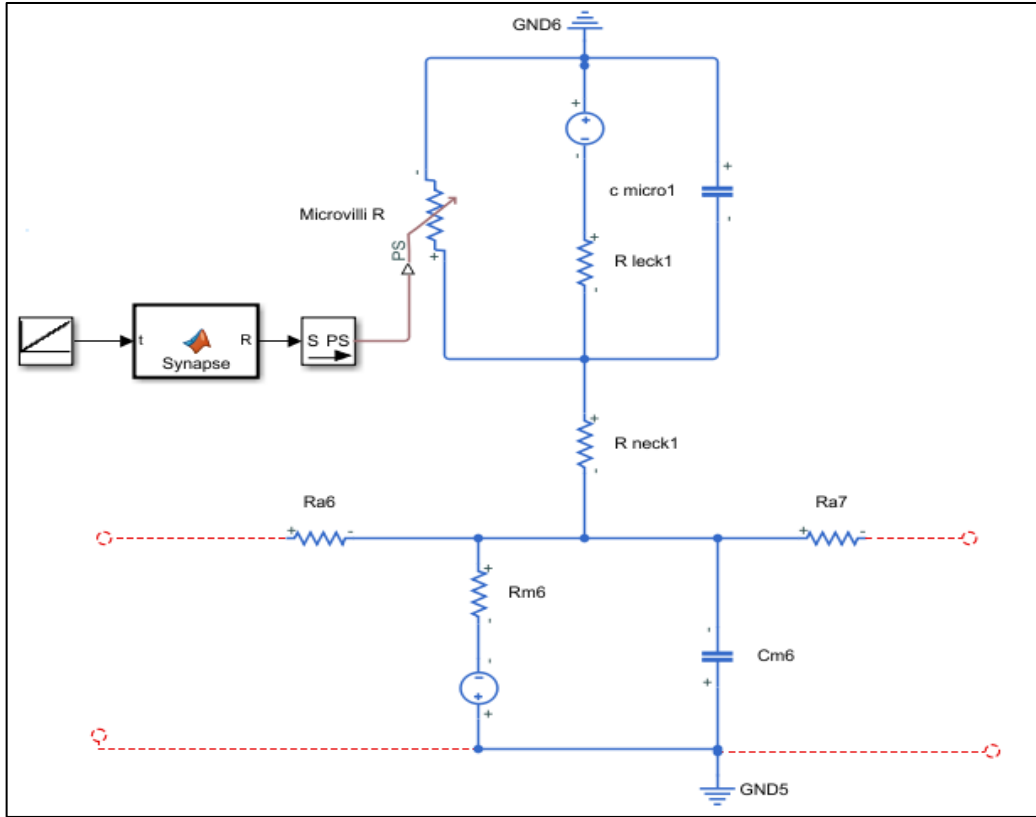
Figure A.7: Somatic segment connected to Microvilli segment.

3) AIS Block:

The AIS block consist of one segment. The AIS block was designed as shown in Figure A.8.
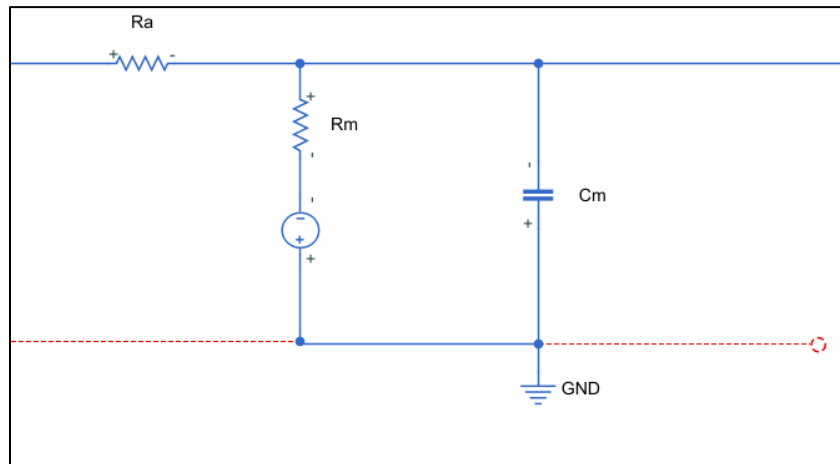
Figure A.8: AIS block.

4) Blocks Connections:

All three blocks were connected as shown in Figure A.9. Vn and Vn1 in Figure A.9 are

voltage sensors which they are used to measure the input and output signals.
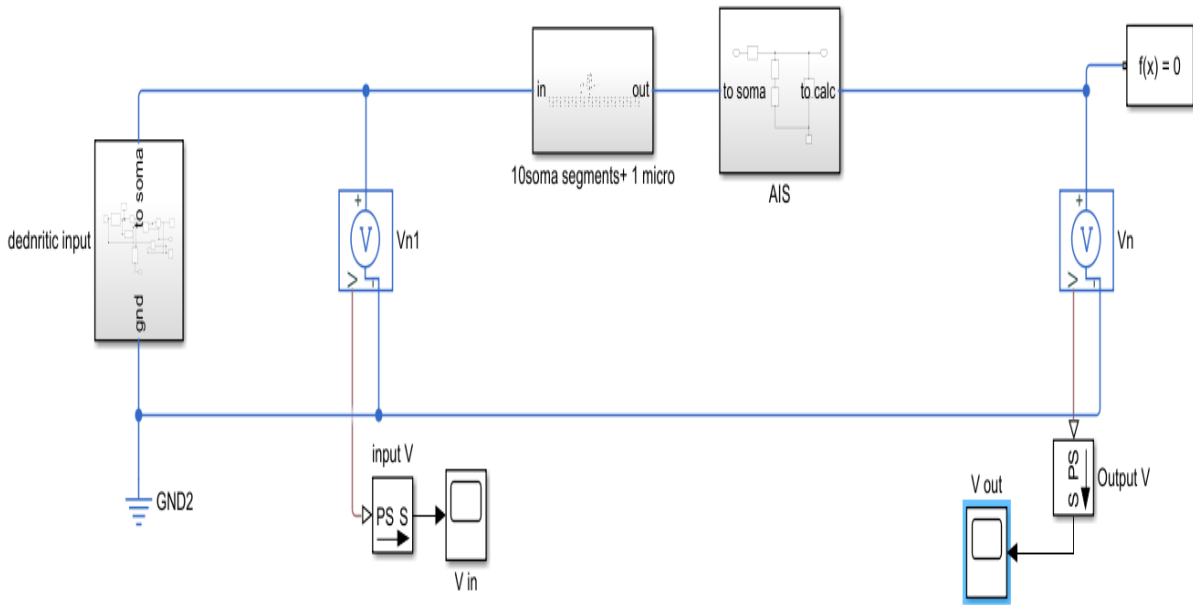
Figure A.9: Circuit block diagram.

Finally, before running the simulation, the variable resistor representing the VGCs

was commented out only for the first simulation. Then, the simulation was run for 100 ms. The

signal was measured at the microvilli (Figure A.10).
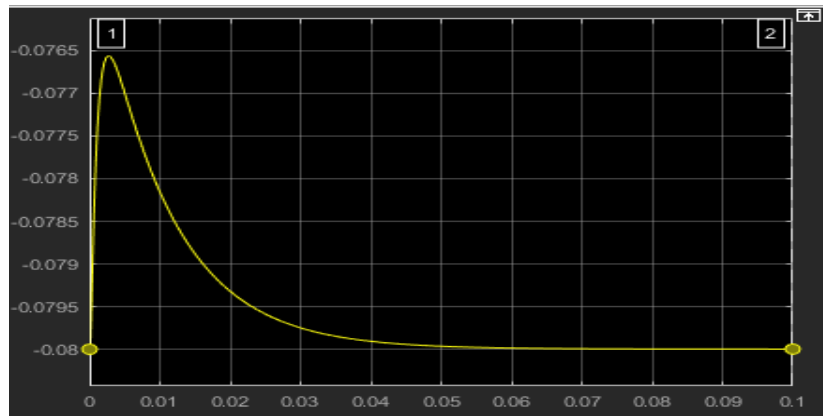
Figure A.10: Output signal at the microvilli with 3.44 mV dendritic input.

For the second simulation in the misfiring experiment, the dendritic input block was commented out as shown in Figure A.11. Then the simulation was run with 10 VGCs on one microvilli and the output signal was measured at the second microvilli. the output signal is shown in Figure A.12.
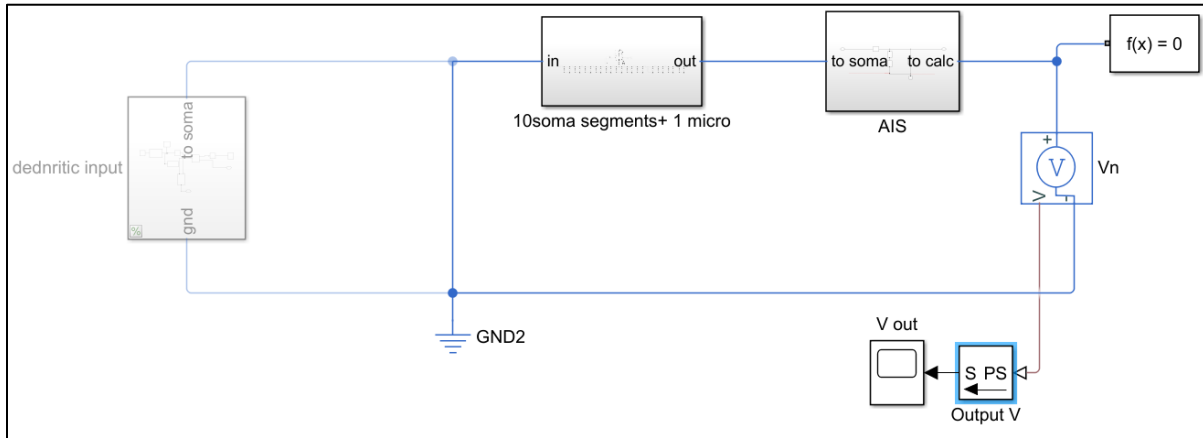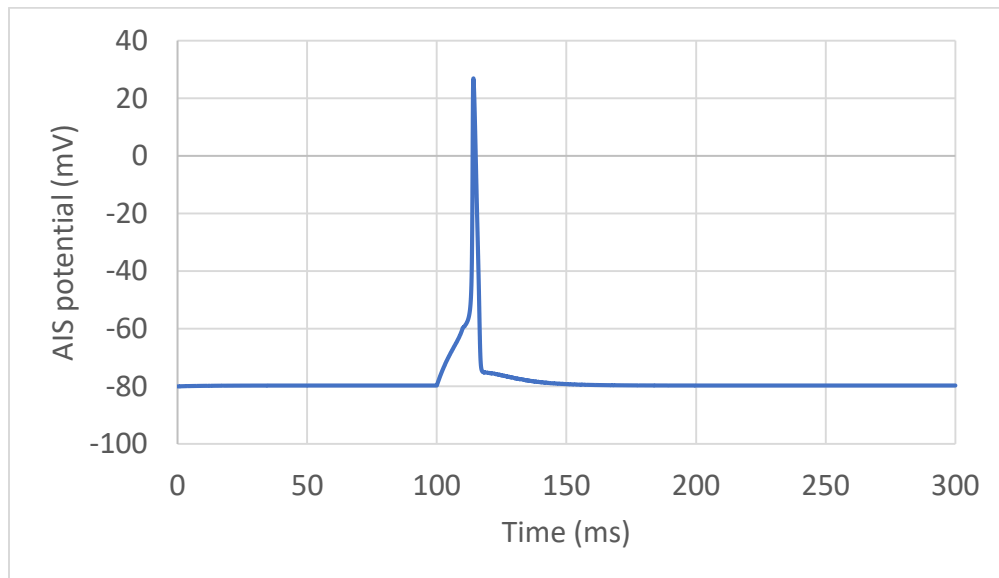

Figure A.11: Second simulation diagram.
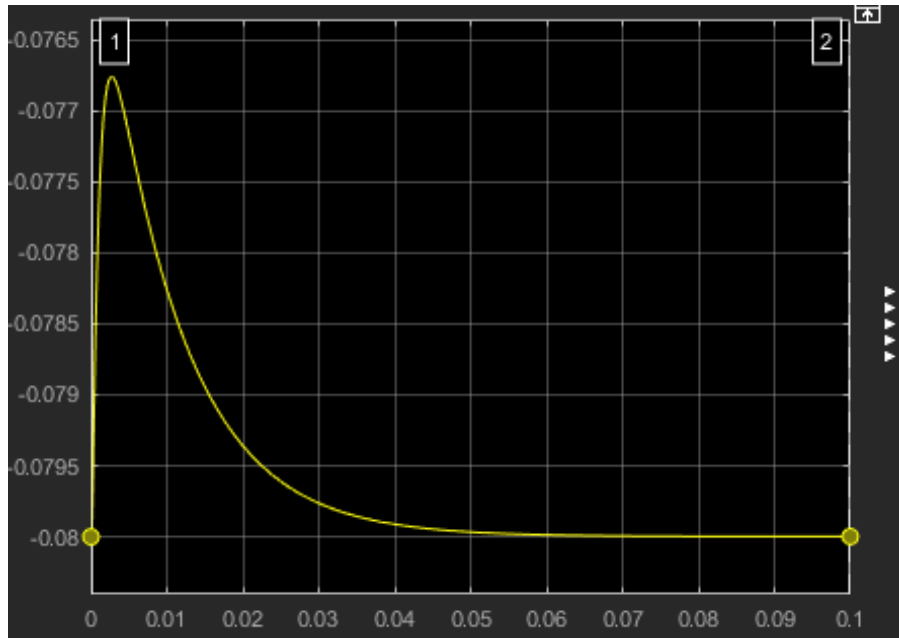
Figure A.12: Output signal at the microvilli.

APPENDIX B: HODGKIN AND HUXLEY MODEL USING NEURON

The output signal at the AIS at different Na$^+$ & K$^+$ VGCs density on soma.
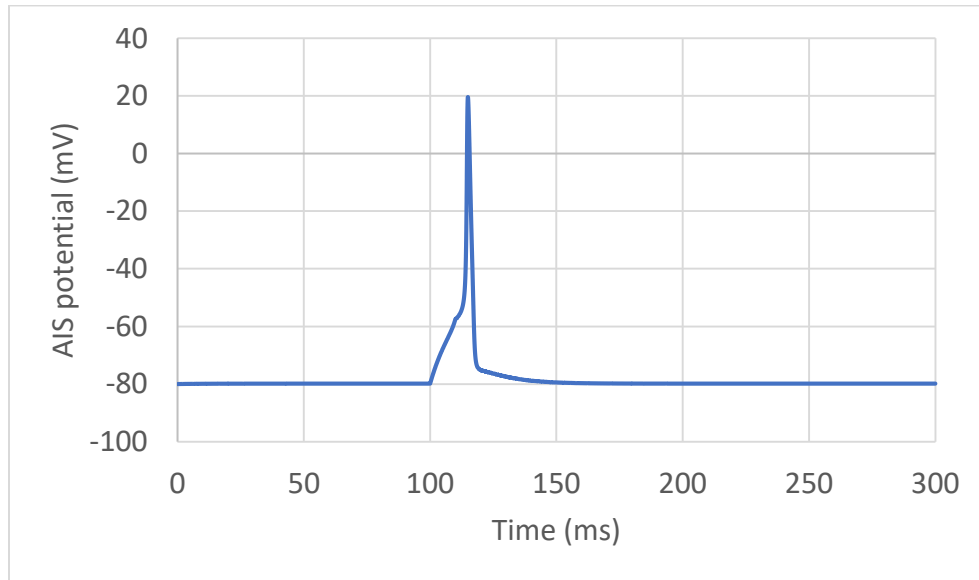
Figure B.1: AIS signal with Na$^+$ VGCs, 40 mS/cm^2, and K$^+$ VGCs, 9 mS/cm^2 on soma.

Figure B.2: AIS signal with Na$^+$ VGCs, 80 mS/cm^2, and K$^+$ VGCs, 18 mS/cm^2 on soma.

The output signal at the AIS with only Na$^+$ VGCs density on soma.
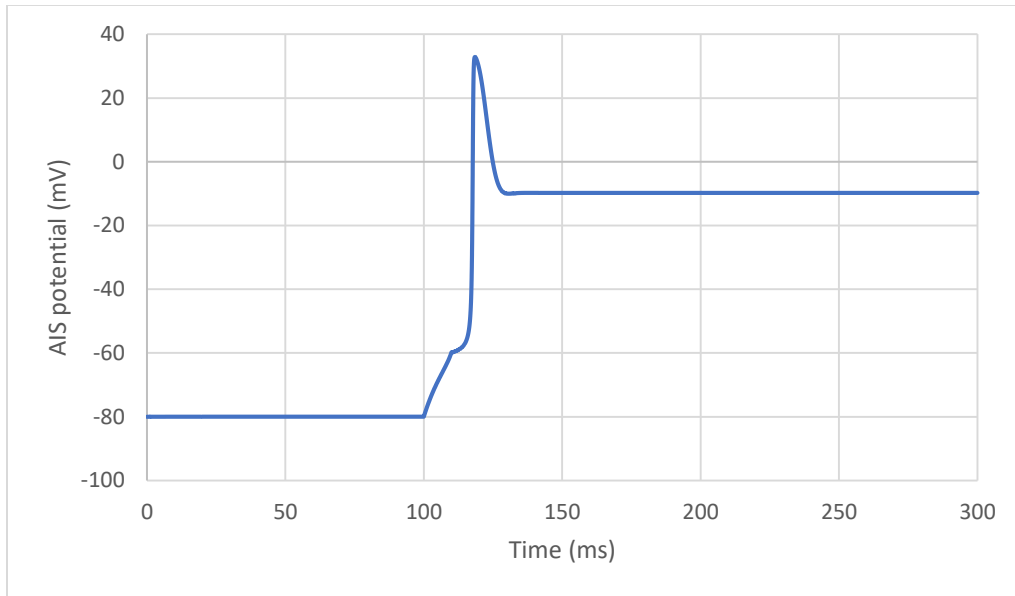
Figure B.3: AIS signal with only Na$^+$ VGCs 40 mS/cm^2 on soma.
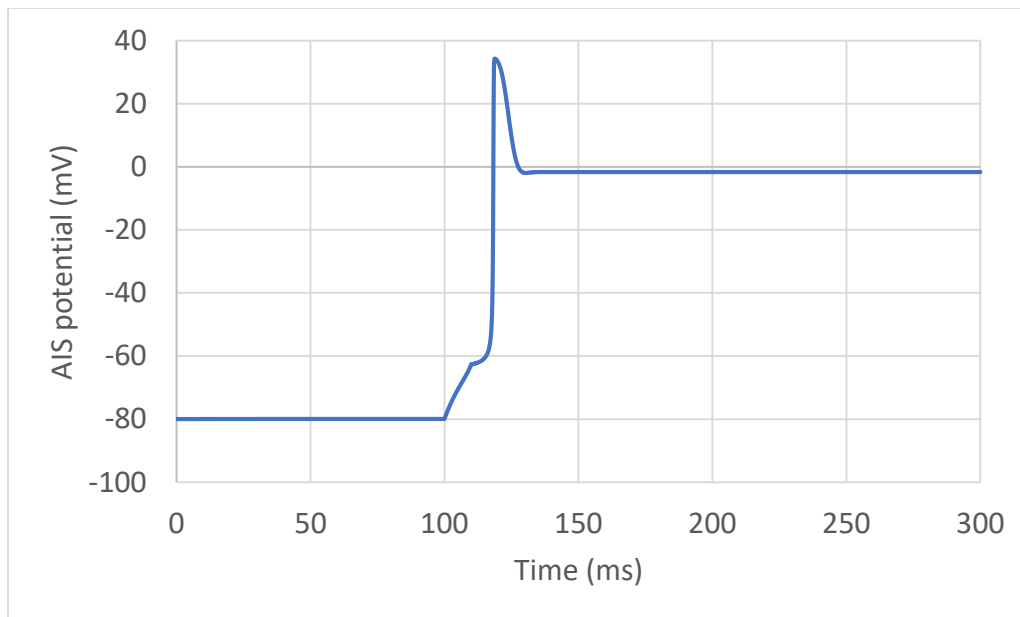
Figure B.4: AIS signal with only Na$^+$ VGCs 80 mS/cm^2 on soma.

The output signal amplitude at the AIS at different Na⁺ & K⁺ VGCs density on microvilli.

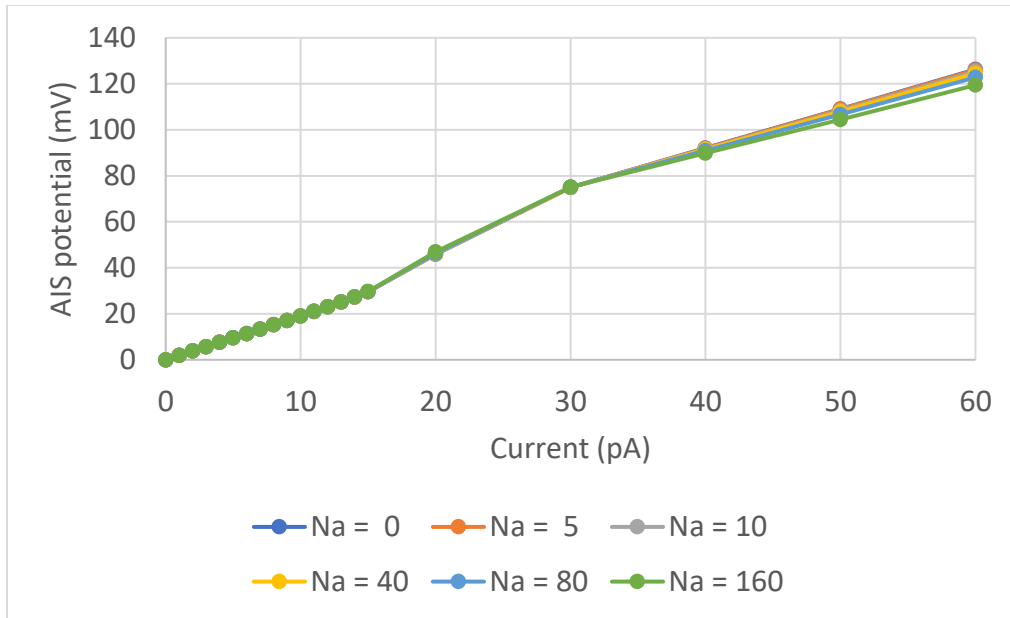**Figure B.5: Signal amplitude at AIS with different Na⁺ & K⁺ VGCs densities (mS/cm²) on microvilli.**

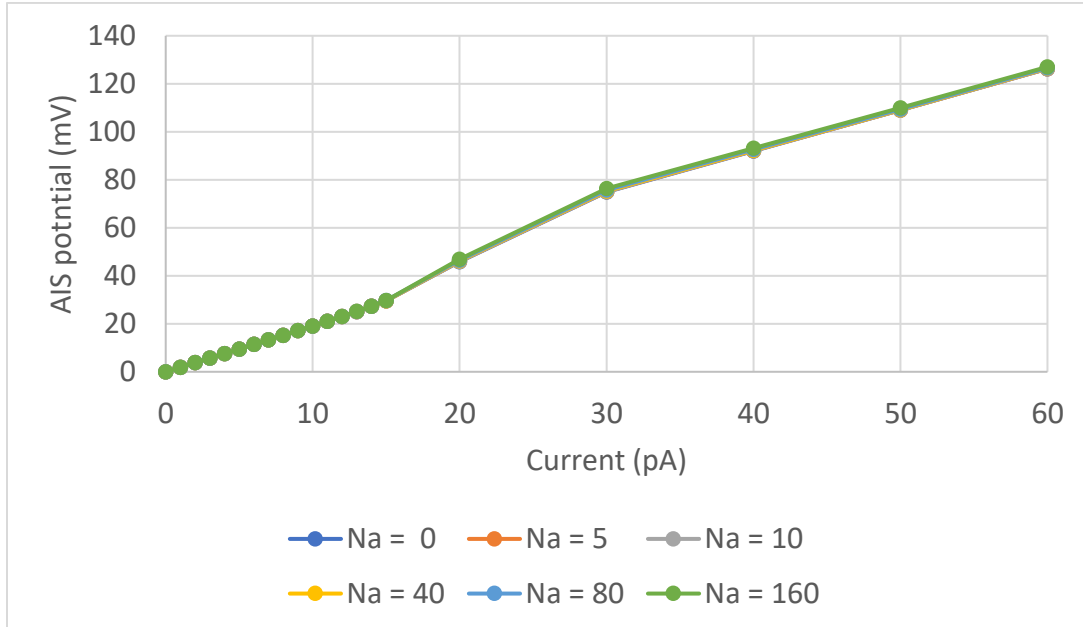**Figure B.6: Signal amplitude at AIS with different Na⁺ VGCs densities (mS/cm²) on microvilli.**

B.1 VGCs on Microvilli experiment using NEURON

A full detailed description of how to design a neuron model can be found in the NEURON

tutorial [50]. The following code was used to simulate the neuron with VGCs located on microvilli.

The VGCs density used in this code was 80 mS/cm^2 Na$^+$ VGCs and 18 mS/cm^2 K VGCs.

```
create soma, axon, dend, microvilli
access dend
connect axon(0), soma(1)
connect dend(0), soma(0)
connect microvilli(0), soma(0.5)
soma {
nseg = 10
diam = 10
L = 10
Ra = 100.0

insert hh

gnabar_hh = 0
gkbar_hh  = 0
gl_hh     = 0.0001
ena    =   35
el_hh = -80
ek     = -75
}

microvilli  {
 nseg = 4
 diam = 0.08
 L = 1
 Ra = 100.0

 insert hh

gnabar_hh = 0.08
gkbar_hh  = 0.018
gl_hh      = 0.0001
ena    =   35
el_hh = -80
ek     = -75
}

axon {
nseg = 1
diam = 1
L = 1
Ra = 100.0

insert hh
```

```
gnabar_hh = 0.15
gkbar_hh = 0.0.018
gl_hh     = 0.0001
ena = 35
ek = -75
el_hh =-80
}

dend {
 nseg = 5
 diam = 5
 L = 1
 Ra = 100.0

insert pas

g_pas = 0.0001
e_pas =-80
}
objectvar stim
dend stim = new IClamp(0.998)
stim.del = 100
stim.dur = 10
stim.amp = 0.01
tstop = 300
```

The Run Control menu in NEURON was used to set the membrane resting potential at –
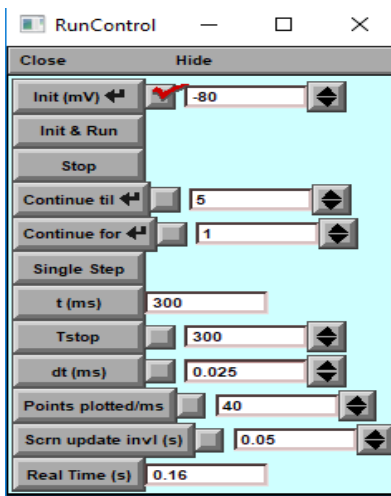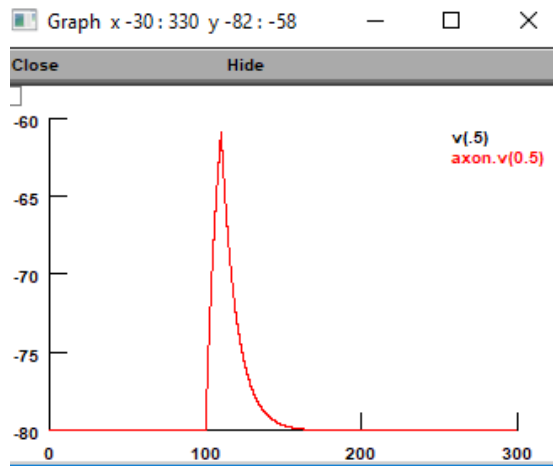
80 mV instead of the default value.

Figure B.7: NEURON run control menu.

From NEURON main menu a voltage graph was chosen to plot the AIS' signal.

Figure B.8: NEURON AIS voltage graph.

From NEURON main menu the data can be exported as Ascii. Under print in the Print & File Window manger, the data can be saved as an Ascii file, which could be opened in Excel, for example, for further analysis.